ELECTRICAL EQUIVALENT MODELING OF THE REVERSE ELECTROWETTING-ON-DIELECTRIC (REWOD) BASED TRANSDUCER ALONG WITH HIGHLY EFFICIENT ENERGY HARVESTING CIRCUIT DESIGN TOWARDS SELF-POWERED MOTION SENSOR

Avinash Gunti

Thesis Prepared for the Degree of

MASTER OF SCIENCE

UNIVERSITY OF NORTH TEXAS

August 2021

APPROVED:

Ifana Mahbub, Major Professor
Kamesh Namuduri, Committee Member
Hua Sun, Committee Member
Shengli Fu, Chair of the Department of Electrical Engineering
Hanchen Huang, Dean of the College of Engineering
Victor Prybutok, Dean of the Toulouse Graduate School

Gunti, Avinash. *Electrical Equivalent Modeling of the Reverse Electrowetting-on-Dielectric (REWOD) Based Transducer along with Highly Efficient Energy Harvesting Circuit Design towards Self-Powered Motion Sensor*. Master of Science (Electrical Engineering), August 2021, 58 pp., 2 tables, 42 figures, 38 numbered references.

Among various energy harvesting technologies reverse electrowetting-on-dielectric energy harvesting (REWOD) has been proved to harvest energy from low frequency motion such as many human motion activities (e.g. walking, running, jogging etc.). Voltage rectification and DC-DC boosting of low magnitude AC voltage from REWOD can be used to reliably self-power the wearable sensors. In this work, a commercial component-based rectifier and DC-DC converter is designed and experimentally verified, for further miniaturization standard 180 nm CMOS process is used to design the rectifier and the DC-DC boost converter.This work also includes the MATLAB based model for REWOD energy harvester for various REWOD models. In REWOD energy harvesting, a mechanical input during the motion causes the electrolyte placed in between two dissimilar electrodes to squeeze back and forth thereby periodically changing the effective interfacial area, hence generating alternating current. The alternating current is given to the rectifier design. There is no realistic model that has been developed yet for this technique. Thereby, a MATLAB based REWOD model is developed for the realistic simulation of the REWOD phenomenon. In the work, a comparison of different REWOD models such as planar surface, rough surface and porous models are performed demonstrating the variations in capacitance, current and voltage.

ACKNOWLEDGEMENT

I would like to express my heartfelt gratitude to Dr. Ifana Mahbub, my major advisor and mentor, for her unwavering support and guidance. Her insights guided me through my academic career at UNT. I was able to push myself to reach goals with the help of Dr. Ifana Mahbub. Hopefully, I would also make her proud.

Dr. Kamesh Namuduri, and Dr. Hua Sun has been invaluable in directing me through my studies and providing useful perspectives.

I am grateful for the Department of Electrical Engineering for awarding me a Teaching Assistantship.

I also would like to thank Dr. Russell Reid from Dixie State University for his support and valuable suggestion.

Finally, I would like to express my gratitude to my co-researchers in the iBioCAS lab for there help, and all of my friends who kept my spirits high throughout my time at UNT.

This material is based upon work supported by the National Science Foundation (NSF) under Grant No. ECCS 1933502.

TABLE OF CONTENTS

Page

ACKNOWLEDGEMENT iii

LIST OF TABLES vi

LIST OF FIGURES vii

CHAPTER 1 INTRODUCTION 1

1.1. Motivation 1

1.1.1. Planar Based REWOD Energy Harvester 2

1.1.2. Rough Surface-Based Energy Harvester 3

1.1.3. Porous based REWOD Energy Harvester 3

1.1.4. AC-DC Boost Converter 4

1.2. Thesis Organisation 4

CHAPTER 2 REVERSE ELECTRO-WETTING-ON-DIELECTRIC 6

2.1. Literature Review 6

2.2. Introduction to REWOD Energy Harvester 8

2.3. MATLAB Implementation of REWOD Model 9

2.3.1. Planar Model MATLAB Implementation 10

2.3.1.1. Results and Simulation 16

2.3.2. Rough Surface-Based REWOD Implementation 19

2.3.2.1. Results and simulation 24

2.3.3. Porous Based REWOD Model Implementation 25

2.3.3.1. Results and Simulation 31

CHAPTER 3 DESIGN OF RECTIFIER USING LTSPICE 35

3.1. Literature Review 35

3.2. Introduction to the Rectifier Design 36

3.2.1. Results and Simulation 37

CHAPTER 4 DESIGN OF RECTIFIER AND DC-DC BOOSTER USING CMOS 180 NM PROCESS 41

4.1. Literature Review 41

4.2. Design Architecture in 180 nm CMOS Process 42

4.3. Simulation Results 45

CHAPTER 5 FUTURE SCOPE AND CONCLUSION 53

REFERENCES 54

LIST OF TABLES

		Page
2.1	Comparison between 3 REWOD model	34
4.1	Performance summary and comparisons	49

LIST OF FIGURES

		Page
1.1	Planar REWOD design	2
1.2	Rough REWOD design	3
1.3	Design for porous REWOD data about the area covered in the hole	4
2.1	Types of energy harvesting chargers	6
2.2	Planar based REWOD energy harvester [**2**]	11
2.3	Lumped element based electrical circuit planar REWOD model	12
2.4	Flow chart/Algorithm for planar & rough surface REWOD model	13
2.5	Voltage source lumped planar REWOD model	14
2.6	Plot between varying height h(t) vs time	16
2.7	Capacitor plot for MATLAB based planar REWOD model	17
2.8	Frequency vs capacitance comparison for planar REWOD model	17
2.9	Comparison Plot between frequency vs planar measured and theoretical voltage	18
2.10	Comparison Plot between frequency vs planar measured and theoretical power	19
2.11	Bottom electrode 3D view for rough surface with extruded cones and pyramids	20
2.12	(a) Cone in rough surface, (b) Flat-headed pyramid in rough surface	21
2.13	Plot between frequency vs simulated and measured voltage for rough surface model	24
2.14	Plot between frequency vs simulated and measure voltage for rough surface model	25
2.15	Plot between simulated and measured power vs frequency for rough surface model	26
2.16	Flow chart/Algorithm for porous REWOD model	27
2.17	Top view of porous REWOD model bottom electrode	28

2.18	Voltage based lumped circuit model for porous REWOD design	29
2.19	Capacitance comparison between MATLAB and measured measurement for porous REWOD model	32
2.20	Voltage comparison between MATLAB and practical measurement	32
2.21	Power comparison plot between MATLAB and measured measurement for porous REWOD model	33
3.1	Full wave rectifier/bridge rectifier	35
3.2	Proposed boost rectifier	37
3.3	Plot between Pin vs Pout and Vin vs Vout	38
3.4	Plot between Pin vs PCE (%)	39
3.5	Plot between Vin vs Vout after REWOD input	39
3.6	Plot between Pin vs Pout and PCE for 38 μm pore diameter	40
3.7	Plot between Pin vs Pout and PCE for 100 μm pore diameter	40
4.1	Block diagram for proposed energy harvesting circuitry	43
4.2	DC-DC Booster	44
4.3	V_{out} vs V_{in} for the proposed rectifier	45
4.4	Voltage conversion efficiency vs. input voltage of the proposed rectifier	46
4.5	PCE vs. P_{in} of the proposed rectifier	47
4.6	V_{out} vs. V_{in} for the rectifier and DC-DC boost converter	48
4.7	VCE vs. Vin of both rectifier and DC-DC boost converter	48
4.8	PCE vs. Pin for rectifier and DC-DC boost converter	49
4.9	Cadence plot between Vin vs Vout after REWOD input	50
4.10	Cadence plot between Pin vs Pout and PCE after REWOD 38 μm pore input	51
4.11	Cadence plot between Pin vs Pout and PCE after REWOD 100 μm pore input	51

CHAPTER 1

INTRODUCTION

1.1. Motivation

The main objective of this project is to design an electrical equivalent model for a self-powered wearable sensor that is in high demand. A wide range of methods can be used to harvest energy using these self-powered wearable sensors, including electromagnetism, thermoelectricity, radio frequency, light (solar), vibration (piezo), etc. Every particular device mentioned above have their own advantages and disadvantages. But, very few of them will operate at very low input frequency signal. During the last few years, the concept of REWOD (reverse electro-wetting-on-dielectric) which is based on mechanical motion energy harvester is introduced. This is in contrast to EWOD (electrical-wetting-on-dielectric) technology, in which electrical energy is converted to mechanical energy. But, REWOD converts mechanical modeling into an electrical signal (AC) hence the term is known as reverse EWOD (REWOD). In general REWOD will converts the mechanical vibrations that has been captured from human motion (eg: walking, jogging, running, etc...) and convert them into an electrical signal which can be used for energy harvesting applications. This REWOD modulates an electrolyte (squeezed repeatedly) between two dissimilar electrodes under an externally applied mechanical force to generate AC current. The AC current is used in some energy harvesting applications hence the low-frequency AC signal is rectified and converted into constant DC voltage.

This work, explores various combinations of electrolyte concentrations, dielectrics, and dielectric thicknesses to generate maximum output power employing a REWOD energy harvester. For the implementation of the fully self-powered wearable sensor, it is necessary to use a zero applied-bias-voltage approach. Thereby, using all the parameters and developing a script that will help in estimating the amount of energy harvested is essential. This electrical equivalent modeling result will help in fabricating the actual REWOD model efficiently.

REWOD will harvest energy from three different types of devices that we studied,

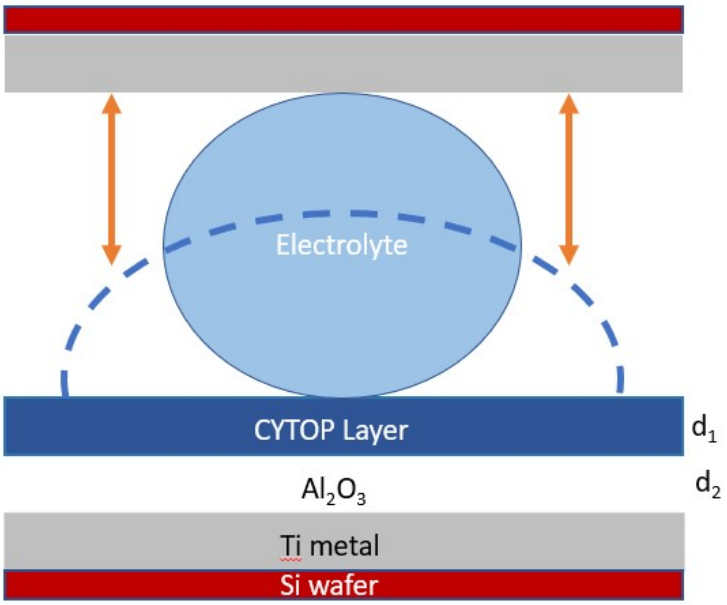

FIGURE 1.1. Planar REWOD design

they are

(i) Planar based REWOD energy harvester

(ii) Rough surface-based REWOD energy harvester

(iii) Porous based REWOD energy harvester

From these three techniques energy is generated and used for few harvesting applications. The objective is to develop a mathematical script for REWOD-based self-powered motion tracking sensors that can be worn and will help in harvesting energy from regular activities. To this end, the proposed rectifier circuits are designed in such a way that the output from the REWOD is rectified and regulated with high power conversion efficiency.

1.1.1. Planar Based REWOD Energy Harvester

In this technique, the electrolyte is placed between two electrodes and squeezes the liquid. Thus the electrodes get conducted by the liquid and thereby AC current is generated. In this technique, the bottom plates is having hydrophobic surface From the fig-1.1 it represents the basic working model of the REWOD design.

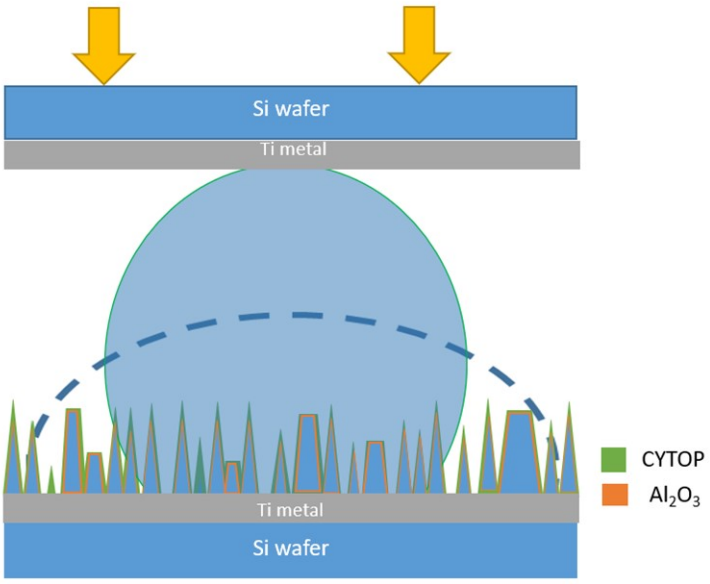

FIGURE 1.2. Rough REWOD design

1.1.2. Rough Surface-Based Energy Harvester

In this rough surface model, the bottom electrode is designed by randomly etching on the surface of the electrode which implies spikes are formed into the surface of the plate. Due to this when the liquid is squeezed in between the two electrodes the area covered by the liquid increases which include the additional area covered by the liquid. Thereby, the capacitor gets charged and energy generated. The methodology is same as planar REWOD model but for this model the inter-facial area covered is more compared to planar REWOD model. Fig-1.2 represents the rough surface REWOD model working. From the figure the area of cones and pyramids included result in higher inter-facial area.

1.1.3. Porous based REWOD Energy Harvester

This porous technique is a bit different from other models. In the porous model, the bottom electrode has pores on the surface and when the liquid is squeezed due to applied pressure, the liquid will goes into the pores in the bottom electrode shown in the fig-1.3 and thereby the electrodes get charged and discharged and from that AC current is generated. Among these three techniques of REWOD harvester porous based energy harvester has highest energy generated and the planar based is having lowest. Hence a MATLAB based

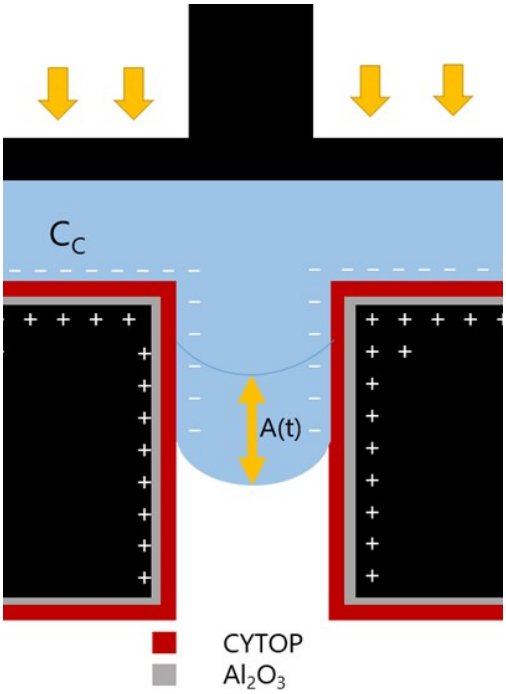

FIGURE 1.3. Design for porous REWOD data about the area covered in the hole

model is designed for all the three REWOD models and compared with other models to know the best model among the three REWOD models.

1.1.4. AC-DC Boost Converter

The measured voltage from the REWOD energy harvester is an AC signal which is having a very low frequency (1-5 Hz).A rectifier needs to be designed for rectifying this low frequency signal into constant DC voltage. Many techniques are available which can rectify an AC signal but, most of them are operated with a high frequency (kHz - MHz) range. This proposed design should operate efficiently at a very low-frequency signal. Hence appropriate design has been developed which can be operated at very low voltage and low frequency. In the end, a DC-DC boost converter is used for constant DC output voltage.

1.2. Thesis Organisation

This thesis is organized as follows. Introduction to REWOD harvesting techniques and AC-DC boost converter (or) rectifier are presented.

Chapter 2 explains the brief concept of REWOD harvester and MATLAB implementation of the three different REWOD models with there simulated results and comparison with measured results.

Chapter 3 discusses the design architecture for rectifier design using commercial components in LTspice and simulation results.

Chapter 4 showcases the simulation results for the proposed design in the 180 nm CMOS process and comparing with other state of the art works.

Finally, the conclusion and future scope are presented in Chapter 5.

CHAPTER 2

REVERSE ELECTRO-WETTING-ON-DIELECTRIC

2.1. Literature Review

Many researchers worked on the self-powered motion sensors and they are widely being used since many decades. Fig: 2.1 describes the different power generators. Hydroelectric energy is used to generate energy from water and turbines. It is also possible to generate energy through solar panels which works when sunlight falls in these solar or photo-volatile (PV) cells and thereby it creates an electric field and then the generated electricity flows to the corners of the plates/panels and into the conductive wires. Similarly, with the help of magnetic field, thermo-electric, piezo-electric (vibration) and radio frequency energy can

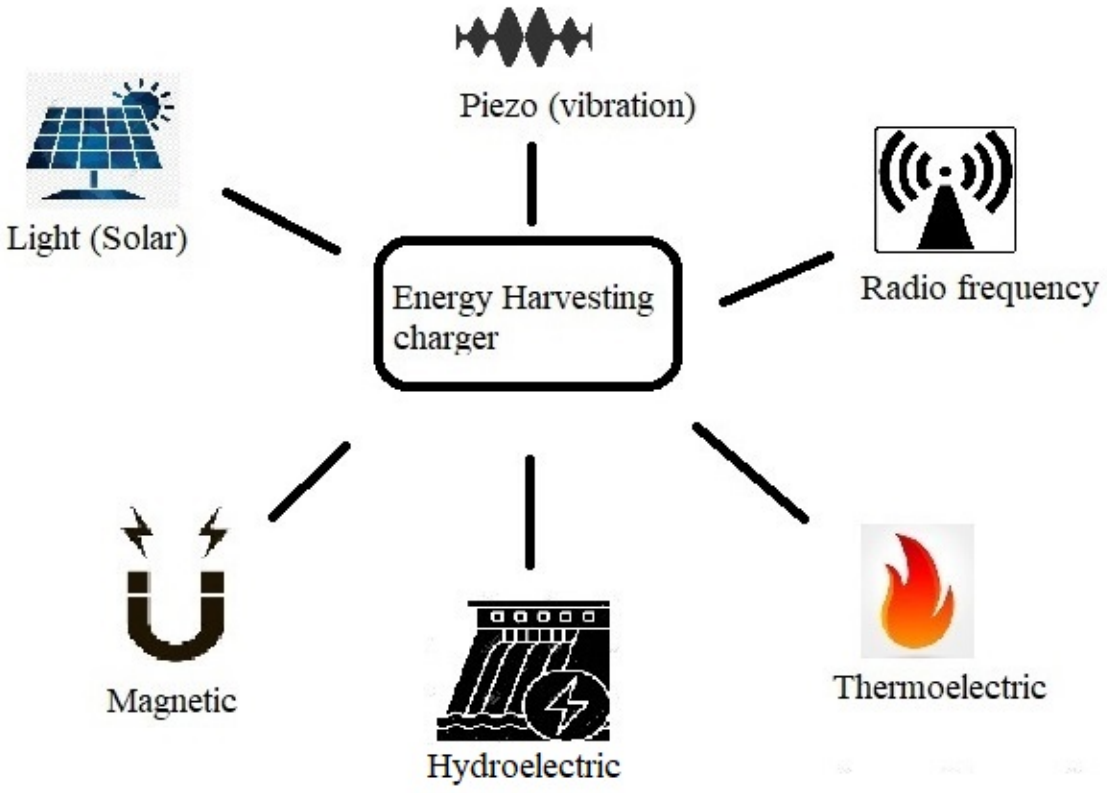

FIGURE 2.1. Types of energy harvesting chargers

be harvested and those techniques are used in different technologies in different public sectors. In this work, REWOD (reverse electro-wetting-di-electric) is used to harvest energy that can be captured from human motion activities and can be used for different harvesting applications.

Portable motion tracking devices have huge demand over the past few years and many techniques have been introduced for self-powered motion sensors that are demonstrated for human health monitoring systems [**5**, **6**, **9**, **11**, **13**]. A wide range of wearable sensing technologies is available, with smartwatches that monitor heart rate and also for human health monitoring and armbands that monitor gesture control [**16**], [**21**], [**23**], [**24**]. The wearable and flexible sensors for user-interactive health-monitoring devices and these flexible electronic device that are lightweight and can be wearable for a person health-monitoring system, [**8**], [**11**], [**5**], [**33**]. For monitoring human bio-signals in a non-invasive manner, highly sensitive, reliable, and suitable for healthcare-monitoring, the wearable sensors based on engineered functional nano/micro-materials with sensing capabilities for detecting electro-physiological vital signs of humans and also have long-term monitoring capability with sustainable power sources [**13**]. To develop self-powered power generators a concept is introduced that is environmentally friendly power generator based on moving liquid dielectric, electrostatic power generator converts mechanical energy into electrical energy by utilizing the principle of a variable capacitance, this proposed device has the utility operating at 1.2 V with a droplet frequency of 6 Hz [**17**]. For health and tactile touch monitoring a wearable microfluidic diaphragm pressure sensor is described by Yuji that explains his potential applications on flexible pressure sensors. Liquid-metal-based sensors are especially undergoing strains of over 200% without fail. The pressure sensor is based on embedded Galinstan microchannels capable of resolving sub-50 Pa change in pressure and sub-100 Pa detection limits and response time of 90 ms is demonstrated [**11**]. There is a technique known as triboelectric nano-generators (TENG) that is implemented which has an effective performance at a low-frequency range (0.25 - 5 Hz) typically known as human motion activity speed [**36**]. The other techniques like piezo-electric, vibration-based, and electromagnetic energy harvesters

are established [**7**], [**37**]. Since piezoelectric energy harvester has been used in various power source applications it is not suitable for self-powered human motion sensors due to its optimal performance. Pointing on these limitations and developing energy harvester from human motion activities which can be operated at a frequency range of 1- 5 Hz with longer lifetime reverse electrowetting-on-di-electric (REWOD) energy harvester is introduced.

In our previous work my colleague worked on planar based REWOD model that achieved an unconditioned REWOD output of 95-240 mV AC generated using a 50 μL droplet of 0.5M NaCl electrolyte and 2.5 mm of electrode displacement from an oscillation frequency range of 1-3 Hz [**1**, **2**]. This work uses commercial off-the-shelf components (COTS) which involves the integrated circuit design of the CMOS process, making it a highly miniaturized system.With 135-240 mV and a forward current of 1 mA the generated converted the AC signal to DC voltage. 3 V DC is measured at the boost converter output, proving the system could function as a self-powered motion sensor. The design is a planar-based model and some other techniques can be more effective in delivering higher output voltage.

A new technique has also been developed for the REWOD generator which is different from the planar surface-based REWOD model. The new transducer is developed with rough-surfaced electrode plate with higher inter-facial area. This harvester is known as the rough surface based REWOD model and there are few works related to this harvester [**38**], [**12**], [**3**], [**20**]. Most of the works/researches are implemented the REWOD harvesters and demonstrated the AC current generated successfully, but very few worked on modeling the design using simulation platforms. For mathematical modeling of these REWOD designs are limited and pointing this and obtaining the novelty in my work by introducing the mathematical design for different models. In this work, a MATLAB-based REWOD harvester is developed for a realistic model that can be used to estimate the amount of energy that can be harvested.

2.2. Introduction to REWOD Energy Harvester

The REWOD technique is developed within the last few years and it is based on mechanical motion energy harvesting. In this design, an electrolyte is rapidly squeezed be-

tween two dissimilar electrodes under an external mechanical force. REWOD is exactly the opposite of EWOD (electro-wetting-on-dielectric). Electro-wetting is a modification of the wetting property for a surface by making it hydrophobic with the help of some applied electric field. So, EWOD is electro-wetting-on-dielectric which converts electrical energy into mechanical energy but, REWOD operated exactly in an opposite way with electro-wetting surface i.e., mechanical energy is converted into electrical energy. This objective is implemented with a fully self-powered wearable sensor which implied zero biased voltage is applied. The electrode layer is designed to use few lumped components that are included with capacitor (variable due to electrolyte varying distance), resistor (including electrolyte), and a current source. Since the basic human activities like running, jogging, and walking when the frequency ranges from 1-5 Hz. REWOD will generate electricity from the motion activities that can be used in some energy harvesting applications.

As discussed the device is implemented with the lumped components which can be calculated practically and theoretically. The designing of the bottom electrode is coated with two different layers, first coated with Al_2O_3 with the thickness (d_1) and dielectric constant (ϵ_1) and the additional layer is CYTOP layer with the thickness (d_2) and dielectric constant (ϵ_2) for surface hydrophobicity. The change in capacitance is due to the mechanical motion of the electrode and with that oscillation of the electrodes the AC current is generated. Based on REWOD modeling different methods are used for energy harvesting using this technique. For realistic simulation, the different model techniques are developed in the MATLAB simulation tool.

2.3. MATLAB Implementation of REWOD Model

The REWOD is developed practically using the electrodes and squeezing the NaCl liquid in between those two electrodes. In fact, 50 μL of liquid NaCl is placed between the electrodes and squeezed by applying some external force. Through this process, the distance between the electrodes changes so, that The area covered by the liquid will change. Proportioning the concept with the capacitor where the charging capacity is depending on

the distance between the electrodes. It is considered that the distance between the electrodes is closer, than the conduction between the electrodes is high due to the higher interfacial area of electrolyte. Correspondingly when the electrodes are farther than the conduction between the electrodes is less. Hereby, charging and discharging take place in the REWOD model, and that current charging and discharging will result in generating an AC signal. The data from the REWOD is an AC signal with a very low-frequency range between 1-5 Hz. When the frequency increases, then, the resultant output also proportionally increases. So, the proposed work is to develop a realistic model that can be used to estimate the amount of energy that can be harvested.

2.3.1. Planar Model MATLAB Implementation

MATLAB is a simulation tool that can be used for different methodologies (e.g.,: signal processing, circuits, image processing, etc.). In this work, MATLAB is used to develop an analytical model for the REWOD design and comparing the results with the fabricated device's measurement results. REWOD is Reverse electro-wetting-on-dielectric, which is an energy-harvesting transducer that can generate energy from the vibration caused by different human motion activities. In this MATLAB model, a script has been developed for a realistic model that can be used to estimate the amount of energy that can be harvested. For the model, it is necessary to develop an appropriate equation for the capacitor, current, and output voltage since the REWOD mechanism is related to charging and discharging due to an electrolyte is squeezed in between two electrodes. As shown in the Fig-1.1 an electrolyte is placed in between two electrodes, when the liquid is squeezed between them, the conduction between the electrodes varies. When the distance between the electrodes varies from 1.5 - 4 mm and when it is at a distance of 1.5 mm then the area covered by the liquid is more, and the conduction between them increases, which imply the charging of the capacitor. Similarly, when the distance is higher, than the area covered by the liquid is less and the capacitor will discharge. The practical planar REWOD model, the bottom electrode is designed with two layers with thickness d_1 (Al_2O_3)=150 nm and d_2 (CYTOP) layer =50 nm, dielectric constants for the layers are ϵ_1=2.1, ϵ_2=9.1 respectively and dielectric constant

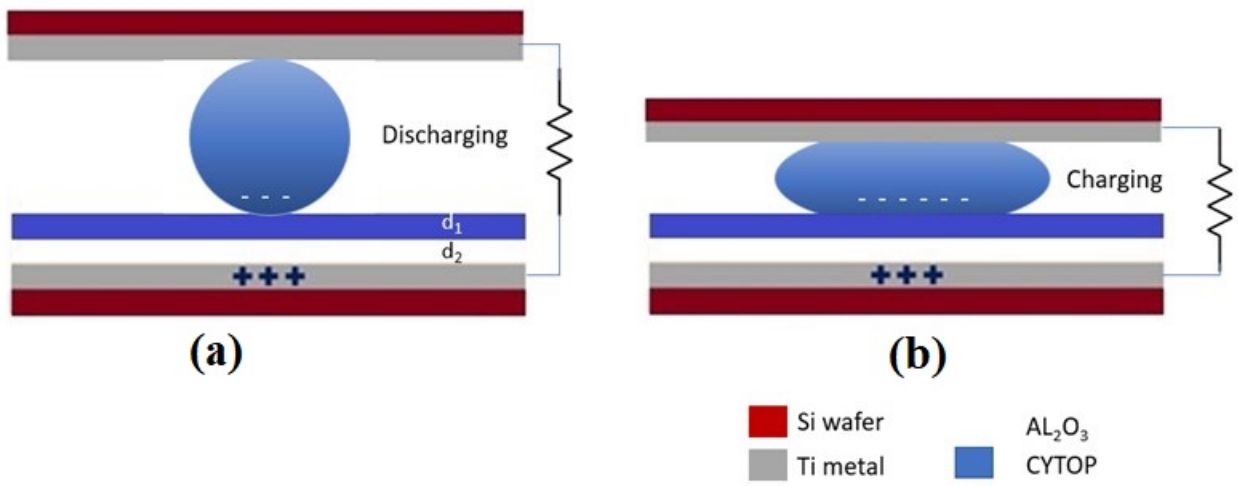

FIGURE 2.2. Planar based REWOD energy harvester [**2**]

for the vacuum (ϵ_0)=$8.85X10^{-12}$ F/m.

The basic REWOD harvester is shown in the fig-2.2 which shows the complete design of the planar REWOD harvester. The same figure clearly shows the two electrodes where the top electrode is coated with highly conductive material titanium (Ti). The bottom electrode is coated with Ti, Al_2O_3, and CYTOP for a higher hydrophobic surface. When the electrodes are set to modulate than the electrode will get sandwiched between the electrode as shown in the second figure in Fig-2.2. So that, the area covered by the liquid is higher comparatively hence charging and discharging takes place.

A circuit is shown in the Fig-2.3 for the REWOD generator as lumped element-based electrical circuit model. For theoretical modeling of the REWOD generator, few equations are derived to estimate the capacitance, voltage, and current. From the Fig-2.3 it represents the REWOD with a parallel resistor and capacitor. When the electrode oscillates at a certain input frequency (f), due to the continuous oscillation of the electrode, an alternating current will be generated through the capacitor. when the electrodes are set to be in motion and the liquid electrolyte (NaCl) is squeezed in between them the interfacial area of the electrolyte varies. Due to the change in area covered by the electrolyte that touches the electrode

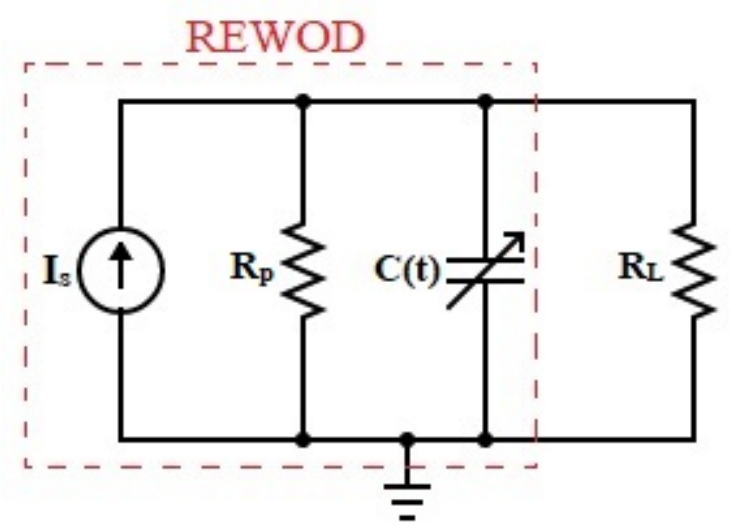

FIGURE 2.3. Lumped element based electrical circuit planar REWOD model

the capacitor will continuously charge and discharges the current. When both electrodes are moving closer than the area covered by the electrolyte is higher and the capacitors will charge and when they are farther the capacitor will discharge. From the practical measurement, the electrolyte is set at a varying height from 1.5 - 4 mm.

A flowchart for the mathematical script implementation is shown in the Fig-2.4 which describes the complete modeling. The first block is initializing block, used to include all the parameters, height varying, volume of the liquid, dielectric constants, dielectric thickness, etc. By using the initialized parameters and the derived formulas for area, capacitance, and voltage and plot them. From the plots, it is possible to estimate the amount of energy harvested from the model. Therefore, the area, capacitance, and voltage derivatives of the following formulas are derived from lumped circuits, and mathematical scripts have been developed for planar and rough models using those equations.

$$C(t) = \frac{\epsilon_0 \epsilon_{eff}.A(t)}{d_1 + d_2} \tag{2.1}$$

From the equation-2.1 C(t) is the varying capacitance, d_1 and d_2 are dielectric thickness of

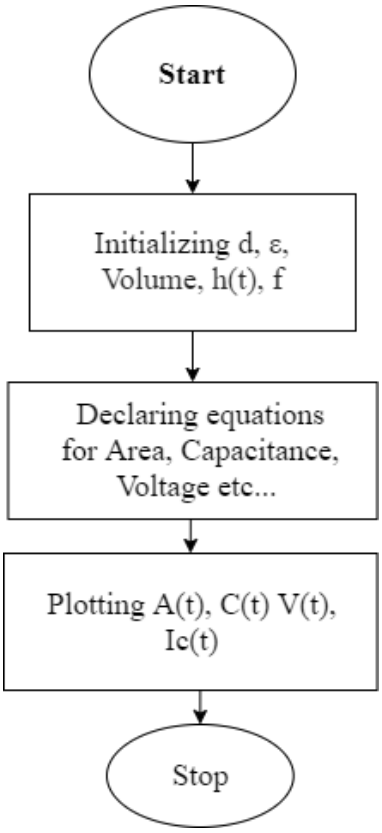

FIGURE 2.4. Flow chart/Algorithm for planar & rough surface REWOD model

Al_2O_3 and CYTOP respectively and ϵ_{eff} is the effective dielectric constant of both layers.

$$\epsilon_{eff} = \frac{d_1 + d_2}{\frac{d_1}{\epsilon_{r1}} + \frac{d_2}{\epsilon_r 2}} \tag{2.2}$$

$$A(t) = \pi r(t)^2 \tag{2.3}$$

In the equation-2.3, A(t) is the area covered by the electrolyte. Estimating that from the top view when the liquid is sandwiched it is considered as a circle. Hence, the area covered is equal to the area of the circle with varying radius. r(t) is the radius of the liquid that covers the electrode. From equation-2.3 we get volume as

$$\begin{aligned} V = A(t)h(t) = \pi r(t)^2 h(t) \\ A(t) = \frac{V}{h(t)} \end{aligned} \tag{2.4}$$

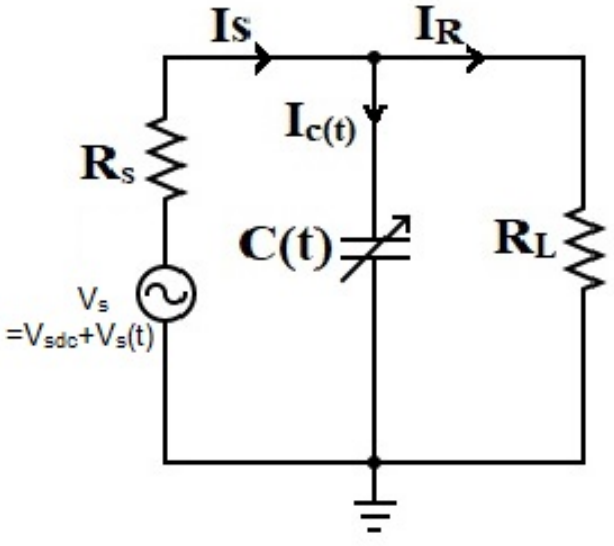

FIGURE 2.5. Voltage source lumped planar REWOD model

From equation-2.3 and 2.4 we get radius r(t) of the liquid that covers the electrode as

$$r(t) = \sqrt{\frac{V}{\pi h(t)}} \tag{2.5}$$

The electrolyte touches the electrodes and form a cylindrical shape. Volume of the cylinder is considered as shown in equation-2.4. V is the volume of the electrolyte, h(t) is the distance between the two electrodes varying from 1.5 - 4 mm and A(t) is area covered by the liquid. For calculating of capacitance area plays the major role. So, using equation-2.3 the capacitance is calculated as

$$C(t) = \frac{\epsilon_0 \epsilon_{eff}(\frac{V}{h(t)})}{d_1 + d_2} \tag{2.6}$$

With the help of the capacitor value it is easy to find the voltage and current across the capacitor. For voltage we consider charge Q(t)= C(t)V and for current $I = \frac{dQ}{dt}$. Using the REWOD lumped circuit the voltage and current equations are derived. So, from the Fig-2.5. This figure is converted from Fig-2.3 where current (I_s) and resistance (R_p) are in parallel to the architecture where resistor (R_s) and voltage ($V_S(t)$) are in series as shown in the Fig-2.5. Using KVL for and KCL rules,we can write

$$V_s = V_{sdc} + V_s(t) \tag{2.7}$$

In the equation-2.7 the source voltage V_s is having both AC component $V_s(t)$ and DC component V_{sdc}.

$$I_s(t) = I_c(t) + I_R(t) \tag{2.8}$$

From the equation-2.8 $I_S(t)$ is the source current, $I_C(t)$ is current through the capacitor $(C(t))$ and $I_R(t)$ is the current across the load resistor (R_L).

The rate of change of charge (dQ) with respect to the time (dt) is known by the current across the capacitor which is specified as,

$$I_c(t) = \frac{dQ(t)}{dt} \tag{2.9}$$

It is known that charge is voltage times of capacitance.

$$Q(t) = C(t)V_{sdc} \tag{2.10}$$

Using the equation-2.10 and 2.9 we get $I_c(t)$ as

$$I_c(t) = V_{sdc}\frac{dC(t)}{dt} \tag{2.11}$$

$$\frac{dC(t)}{d(t)} = \frac{\epsilon_0\epsilon_{eff}V}{d_1 + d_2}(\frac{-1}{h(t)^2}) \tag{2.12}$$

$$I_R(t) = \frac{V(t)}{R_L} \tag{2.13}$$

$$I_S(t) = \frac{V_s}{Z(t)} \tag{2.14}$$

$$Z(t) = R_s + Z_1(t) \tag{2.15}$$

In the equation-2.15 Z(t) is the series connection of Z_1 and R_S.

$$Z_1(t) = X_{C(t)}||R_L = \frac{X_C(t)R_L}{X_C(t) + R_L} \tag{2.16}$$

In the equation-2.16 $Z_1(t)$ is parallel resistance of $X_C(t)$ and R_L.

$$X_{C(t)} = \frac{1}{2\pi f C(t)} \tag{2.17}$$

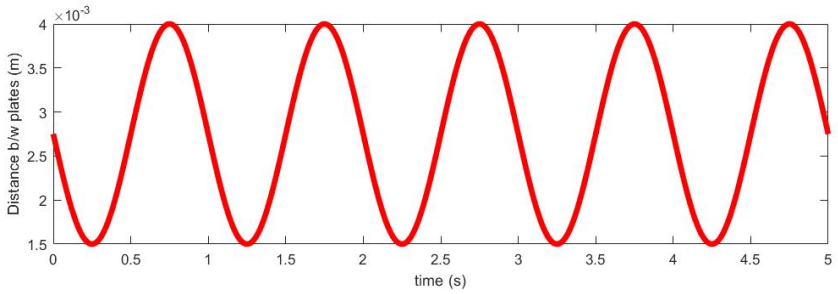

FIGURE 2.6. Plot between varying height h(t) vs time

From equation-2.17 f is the frequency of the moving electrodes which is captured from the human motion.

$$I_S(t) = \frac{V(t)}{Z_1(t)} = I_C(t) + I_R(t) \tag{2.18}$$

$$V(t)(\frac{1}{Z_1(t)} - \frac{1}{R_L}) = V_{sdc}\frac{dC(t)}{dt} \tag{2.19}$$

From equation-2.19 V(t) is the AC voltage varies due to varying capacitance and V_{sdc} is the constant biased voltage form the source voltage V_S.

$$V(t) = \frac{V_{sdc}\frac{dC}{dt}}{\frac{1}{Z_1(t)} - \frac{1}{R_L}} \tag{2.20}$$

There by, voltage derivation for REWOD planar model is derived using lumped circuit. This voltage is used to implement the MATLAB code and compute the voltage at different input frequency ranges from 1-5 Hz.

2.3.1.1. Results and Simulation

With the help of MATLAB script, a planar-based REWOD model was developed. Using all the parameters including dielectric thickness, dielectric constant, volume of the liquid and few other parameter, the plot for capacitor, voltage and power are plotted. The height is varied from 1.5 - 4 mm distance, and the height changes with the frequency. In the script the height is declared as sine signal as shown in Fig-2.6, the frequency is given as a sine signal input. Using the height and the derived equations for plotting the capacitance, voltage, and power.

The capacitor output shown in the Fig-2.7 which is varied from 3.0 - 5.7 nF It can be seen that the increase in height proportionally reduces the capacitance, and vice versa. And in

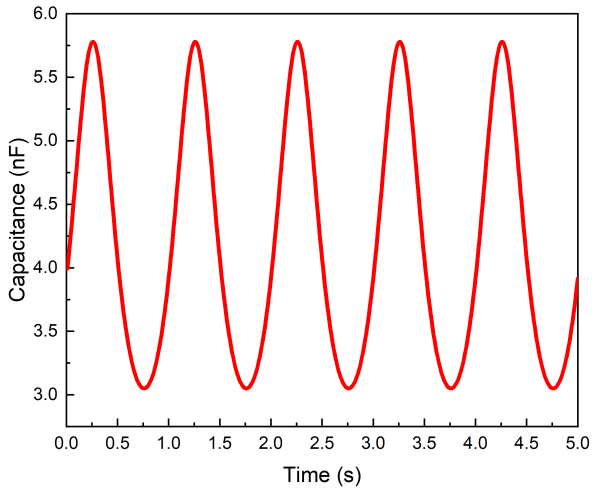

FIGURE 2.7. Capacitor plot for MATLAB based planar REWOD model

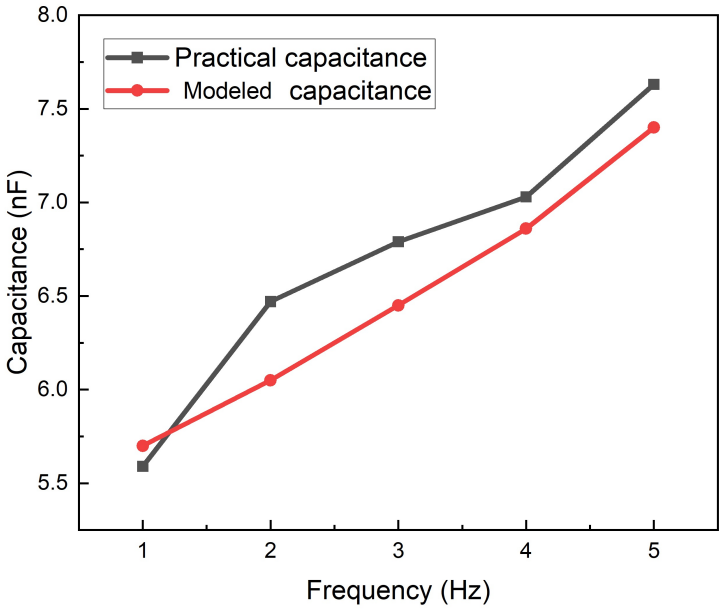

FIGURE 2.8. Frequency vs capacitance comparison for planar REWOD model

the Fig-2.8, this is a graph used to compare the measured capacitance with the theoretical measured value. The measured capacitance and the theoretical capacitance almost match. By using the equation-2.21 to calculate the error between the two graphs, the error at 5 Hz

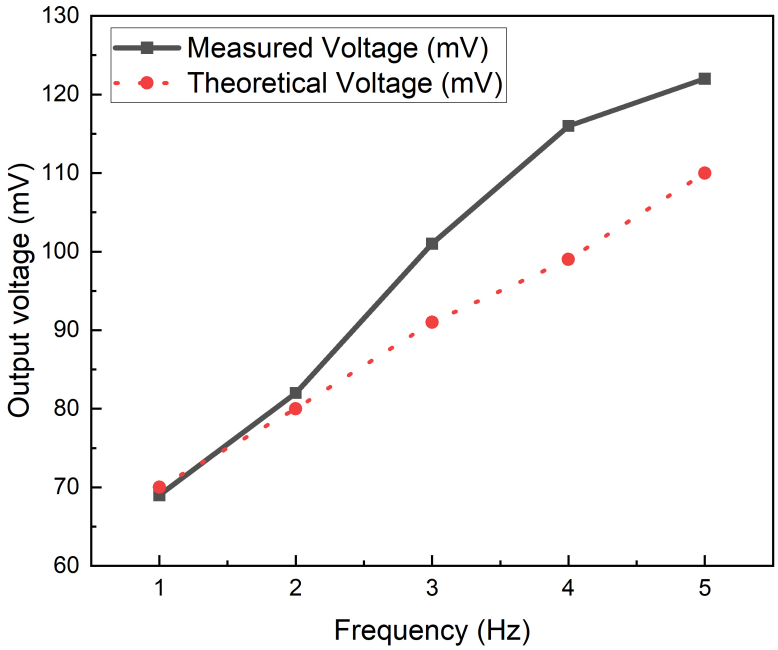

FIGURE 2.9. Comparison Plot between frequency vs planar measured and theoretical voltage

is close to 3.8%. The average error of the capacitor is 3.1%, which means that the accuracy is close to 97%.

$$Error(\%) = \frac{Simulated\_value - practical\_value}{practical\_value} X100\% \tag{2.21}$$

Similarly, the voltage comparison is shown in the Fig-2.9, the voltage range is 70-110 mV with 1 - 5 Hz respectively. Using the equation 2.21, the average error of the planar sample voltage is 8.8%, which means that the accuracy of the voltage is close to 91%. Similarly, it can be seen from Fig-2.10 that it represents the comparison curve between the measured power and the theoretical power and frequency. Its average power is 4.66 nW. And using the equation-2.21 to calculate the error rate with the measured power, the error rate is close to 20%, which means 80% accuracy.

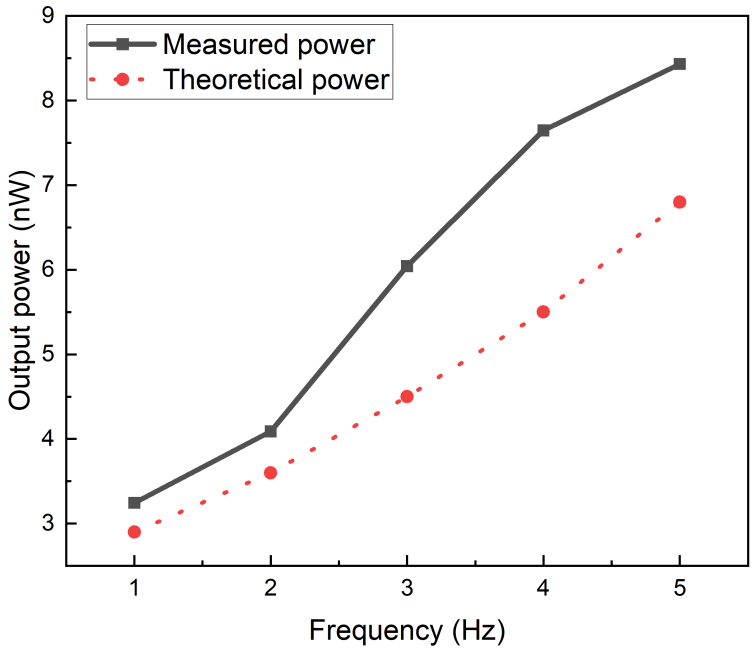

FIGURE 2.10. Comparison Plot between frequency vs planar measured and theoretical power

2.3.2. Rough Surface-Based REWOD Implementation

In view of some of the limitations of the planar REWOD model, a rough surface REWOD model is implemented, which has a higher interfacial area than the planar-based REWOD model. The method is similar except for the difference is in the rough surface modeling. The silicon wafer is randomly etched so that spikes are formed at the top of the layer. These spikes are considered to be different numbers of cones and flat-headed pyramids. Since the cone and pyramids are squeezed on the plate, this will help increase the area covered by the liquid. My colleague worked on counting the number of cones and pyramids using SEM image. By considering the length of 9.5 μm and the width of 12.5 μm, which is a small part of the electrode using the SEM image. Considering the area of the part is 118.75 μm^2, there are 117 cones and 5 pyramids. Therefore, this method can be used to flexibly calculate the number of cones and flat headed pyramids covered when the

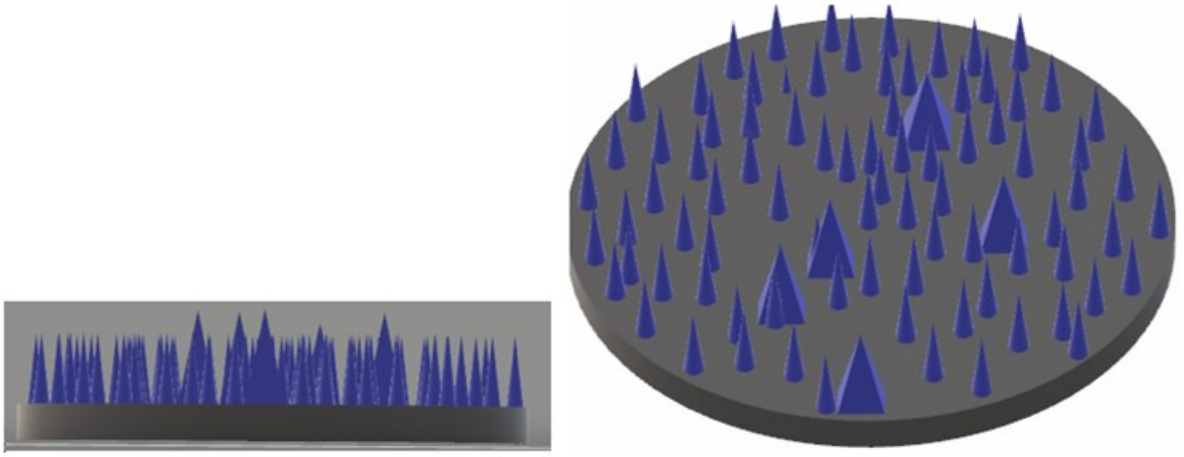

FIGURE 2.11. Bottom electrode 3D view for rough surface with extruded cones and pyramids

electrolyte is squeezed. In the same way height is measured using profilometer. The surface of the electrode after the etching is as shown in the Fig-2.11. The total area is considered as the area covered by the plane surface, the surface area of the cone excluding the cone base area, the area covered by the top surface of flat head of the pyramid, and finally the surface area of the flat-headed pyramid without the base area. This rough surface is measured in 3 different ways (i) Bottom electrode is rough, (ii) Top electrode is rough, and (iii) Both the top and the bottom electrodes are rough. In these top and bottom rough electrodes, due to the large interface area, they have a higher output. For the following two electrodes with rough surfaces, the area covered by the electrolyte can be obtained by the following formula. A MATLAB script was developed for this area specification. These equations are declared in the code that will calculate the area covered by the liquid and the variable capacitance.

Consider the cone whose radius is r_c, height is h_c, and L is the tilt height as a reference, and its representation is shown in Fig- 2.12(a). For the liquid squeezed between the electrodes, the liquid covers the surface area of the liquid other than the base area.

The lateral surface area of the cone (A_c) is given by

$$A_c = \pi r_c \sqrt{(h_c^2 + r_c^2)} \tag{2.22}$$

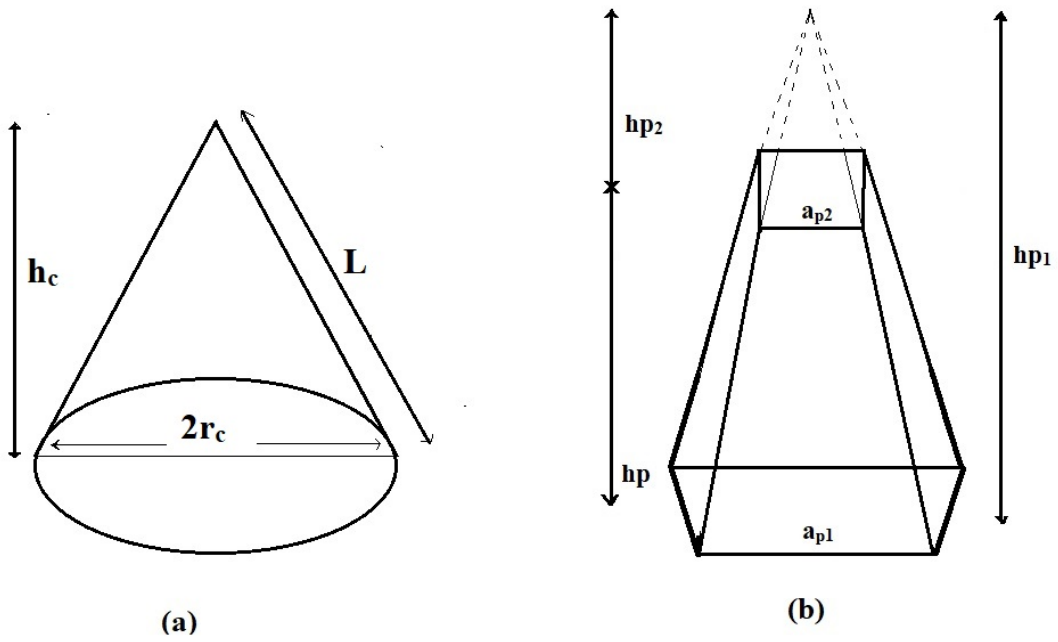

FIGURE 2.12. (a) Cone in rough surface, (b) Flat-headed pyramid in rough surface

Base area of the cone (A_{bc}) is given by

$$A_{bc} = \pi r_c^2 \tag{2.23}$$

Similarly for flat headed pyramid as shown in the Fig-2.12(b) the base area of flat headed pyramid is A_{b_p}

$$A_{bp} = a_{p_1}^2 \tag{2.24}$$

And for area of top head of the pyramid is A_{t_p}

$$A_{tp} = a_{p_2}^2 \tag{2.25}$$

In the equation-2.24 & 2.25 a_{p_1} and a_{p_2} are base length and top length of the flat headed pyramid respectively. The lateral surface area of the pyramid that is used in the design is given as A_p.

$$A_{tp} = 2a_{p_1}\sqrt{\frac{a_{p_1}^2}{4} + h_{p_1}^2} - 2a_{p_2}\sqrt{\frac{a_{p_2}^2}{4} + h_{p_2}^2} \tag{2.26}$$

From the equation-2.22 & 2.26 lateral surface area of cone and pyramid is derived. This area is used for capacitance modeling, and the capacitance is used to calculate the voltage and current for rough surface modeling. For the considered region of the plate of side length of 12.5 μm and width 9.5 μm the modeled area is 118.75 μm^2. So using this the total area (A_T) is given as

$$A_T = MA + N_c(A_c - A_{bc}) + N_p(A_p + A_{tp} - A_{bp}) \tag{2.27}$$

In the equation-2.27 is N_c and N_p are number of cones and pyramids respectively at particular portion area. Hence the total capacitance for the rough surface model is

$$C(t) = \frac{\epsilon_0 \epsilon_{eff} A_T}{d_1 + d_2} \tag{2.28}$$

Therefore, the capacitance is known, and in order to find the voltage and current on the capacitance, the rate of change of the capacitance is required. Except for the total area (A_T), all parameters are time independent. So, to find dC(t) it is necessary to find the rate of change of total area (dA_T).

$$\begin{aligned} \frac{dA_T}{dt} &= \frac{d}{dt}(MA + N_c(A_c - A_{bc}) + N_p(A_p + A_{tp} - A_{bp})) \\ &= \frac{dN_c}{dt}(A_c - A_{bc}) + \frac{dN_p}{dt}(A_p + A_{tp} - A_{bp}) \end{aligned} \tag{2.29}$$

From the measured data it is known that the area is 118.75 μm^2. At that area there are 117 cones and 5 flat headed pyramids. Using this we can find total number of cones and pyramids that are covered by the electrolyte.

$$\begin{aligned} A_{total} &= \frac{Volume}{h(t)} \\ \frac{dA_{total}}{dt} &= \frac{Volume}{\pi}(\frac{-1}{h(t)^2}) \end{aligned} \tag{2.30}$$

The equation-2.30 is the area covered by the electrolyte but this is excluding the cones and pyramids.

$$\begin{aligned} T_{N_c} &= 117(\frac{A_{total}}{118.75 * 10^{-12}}) \\ T_{N_p} &= 5(\frac{A_{total}}{118.75 * 10^{-12}}) \\ \frac{dT_{N_c}}{dt} &= (\frac{117}{118.75 * 10^{-12}})\frac{dA_{total}}{dt} \\ \frac{dT_{N_p}}{dt} &= (\frac{5}{118.75 * 10^{-12}})\frac{dA_{total}}{dt} \end{aligned} \tag{2.31}$$

T_{N_C} and T_{N_p} total number of cones and total number of flat-headed pyramids respectively that is in contact with the electrolyte.

Equation-2.27 is the area at specific portion, that has been considered for the measure number of cones and pyramids. The actual area of the electrolyte is A(t) and its equation is

$$A(t) = A_{total} + T_{N_c}(A_c - A_{bc}) + T_{N_p}(A_p + A_{tp} - A_{bp}) \tag{2.32}$$

$$\begin{aligned} \frac{dA(t)}{dt} &= \frac{d}{dt}(A_{total} + T_{N_c}(A_c - A_{bc}) + T_{N_p}(A_p + A_{tp} - A_{bp})) \\ \frac{dA(t)}{dt} &= \frac{dA_{total}}{dt} + \frac{dT_{N_c}}{dt}(A_c - A_{bc}) + \frac{dT_{N_p}}{dt}(A_p + A_{tp} - A_{bp})) \end{aligned} \tag{2.33}$$

The rate of change in total area is used for calculation of voltage and current which depends on the rate of change of capacitance (dC(t)/dt).

$$\frac{dC(t)}{dt} = \frac{\epsilon_0 \epsilon_{eff}}{d_1 + d_2}\frac{dA(t)}{dt} \tag{2.34}$$

By substituting equation-2.33 in 2.34 we get the rate of change of capacitor and dC(t)/dt is used in the voltage equation to calculate the output voltage from the rough surface REWOD model.

$$V(t) = \frac{V_{sdc}\frac{dC(t)}{dt}}{\frac{1}{Z_1(t)} - \frac{1}{R_L}} \tag{2.35}$$

$$I_c(t) = V_{sdc}\frac{dC(t)}{dt} \tag{2.36}$$

These mathematical derivations are used in the MATLAB code for simulating the realistic response from the rough surface based REWOD energy harvester.

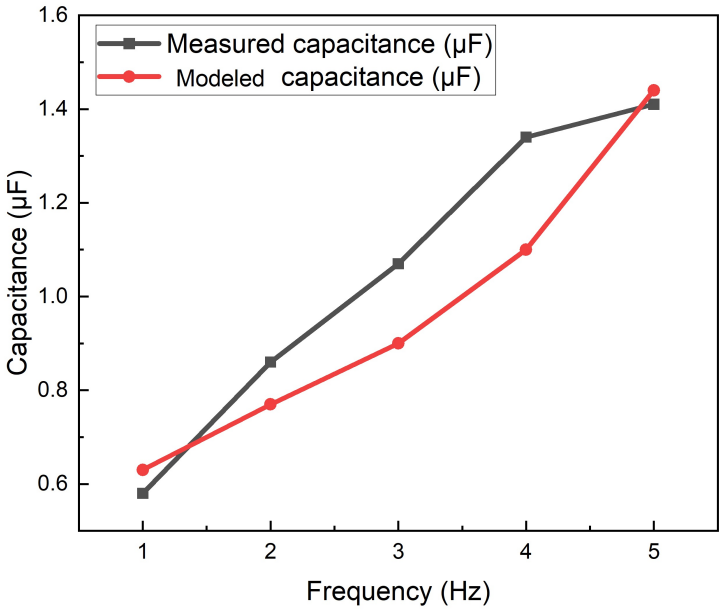

FIGURE 2.13. Plot between frequency vs simulated and measured voltage for rough surface model

2.3.2.1. Results and simulation

From Fig- 2.13, it can be seen that the comparison table of theoretical capacitance and measured capacitance. According to the MATLAB simulation, the capacitance range of the rough surface model is close to 0.6-1.4 μF, and almost matches the measured capacitance. When calculating the error using the equation between the measured capacitance and the simulated capacitance 2.21, at a frequency of 5 Hz, the error is 3.6%, and at 1 Hz, the error is 3.3%. The average error of the capacitor is close to 3%, or 97% accuracy.

From the plot as shown in the Fig-2.14, the comparison between measured and simulated voltage is represented. From the simulation plot, it is seen that the voltage range varies from 100 - 215 mV. Calculating the error with simulation and measured voltage the average error using equation-2.21 is 11% that implies the accuracy is 89%.

From the Fig-2.15 that represents the comparison between simulated and measured power for the rough surface model, the average power gained is 54.5 nW and the average error with

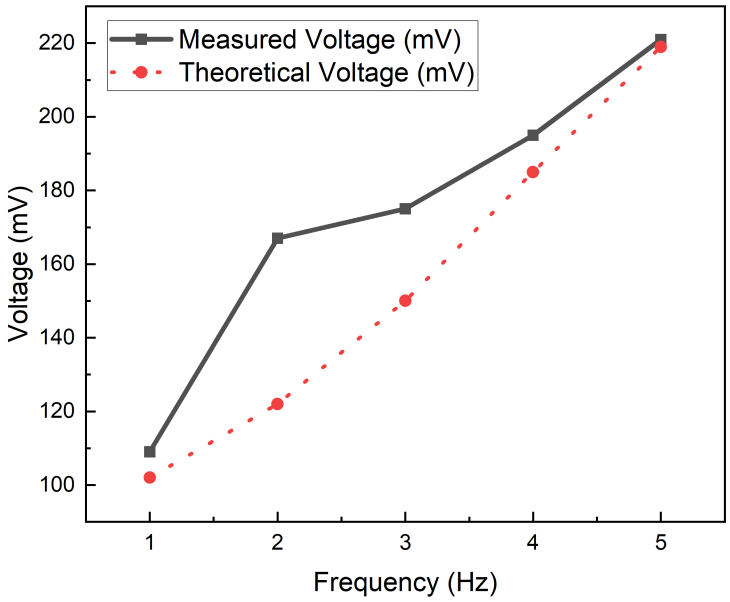

FIGURE 2.14. Plot between frequency vs simulated and measure voltage for rough surface model

measured power is nearly 15% i.e. 85% accuracy.

2.3.3. Porous Based REWOD Model Implementation

The porous REWOD model is another harvest model technology, which is more effective and reliable than the planar model and the rough model. The design of the electrodes is completely different from the other models. On a planar surface, the area covered by the electrolyte is very small and the power output is also very low. Hence, rough electrode is designed and for the rough surface model, etching the silicon wafer so that spikes will be extruded from the surface so that the interfacial area covered by the electrode is higher so that the power outcome is high comparatively. In this porous REWOD modeling, the liquid is squeezed between two electrodes, but the bottom electrode should be designed in such a way that there are many holes in the bottom electrode. Therefore, when the top electrode is set to oscillate at a frequency of 1-5 Hz, it is a normal human movement activity (for example: walking, running, jogging, etc.). The liquid goes in and out into those pores such

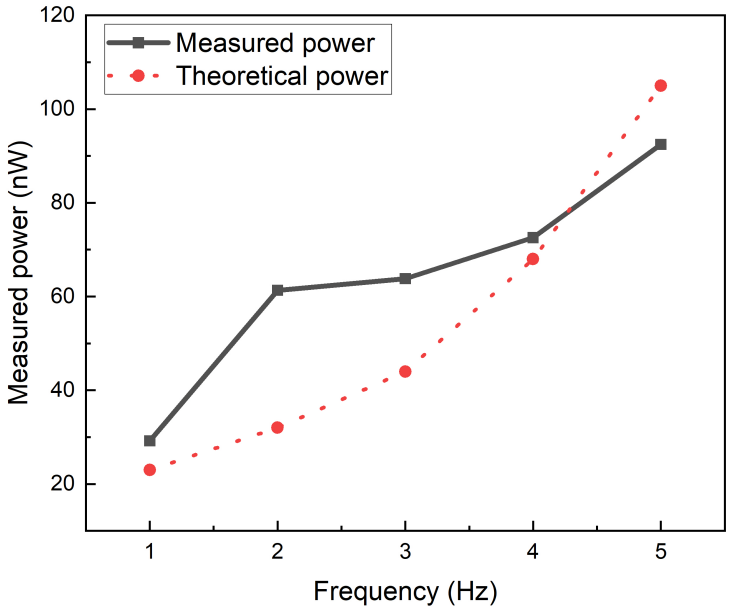

FIGURE 2.15. Plot between simulated and measured power vs frequency for rough surface model

that the pore area is also included when squeezed along with the planar area. The conduction area is covered in two ways, the constant area which is a non-porous area of the liquid that touches a particular portion of the electrolyte constantly, and the variable area which is the area of pores that liquid goes in and out in the bottom electrode. If considering one pore between 'n' number of pores in the bottom electrolyte and determining the area covered by that liquid. The hole area is considered as the surface area of the cylinder, and the height changes by changing the depth of the liquid covered during the modulation process, as shown in Fig-1.3. Due to the change in the area, the capacitance also varies respectively (C α A). Based on different requirements different bottom electrodes are considered which have different pore diameters. In this design, the considered diameters are 38μm and 100 μm. A small figure is shown in Fig-2.17 that represents how the pores are when seen from the top view of bottom electrode. By using all these parameters including the number of pores, dielectric thickness, dielectric constants for this model and developing a MATLAB

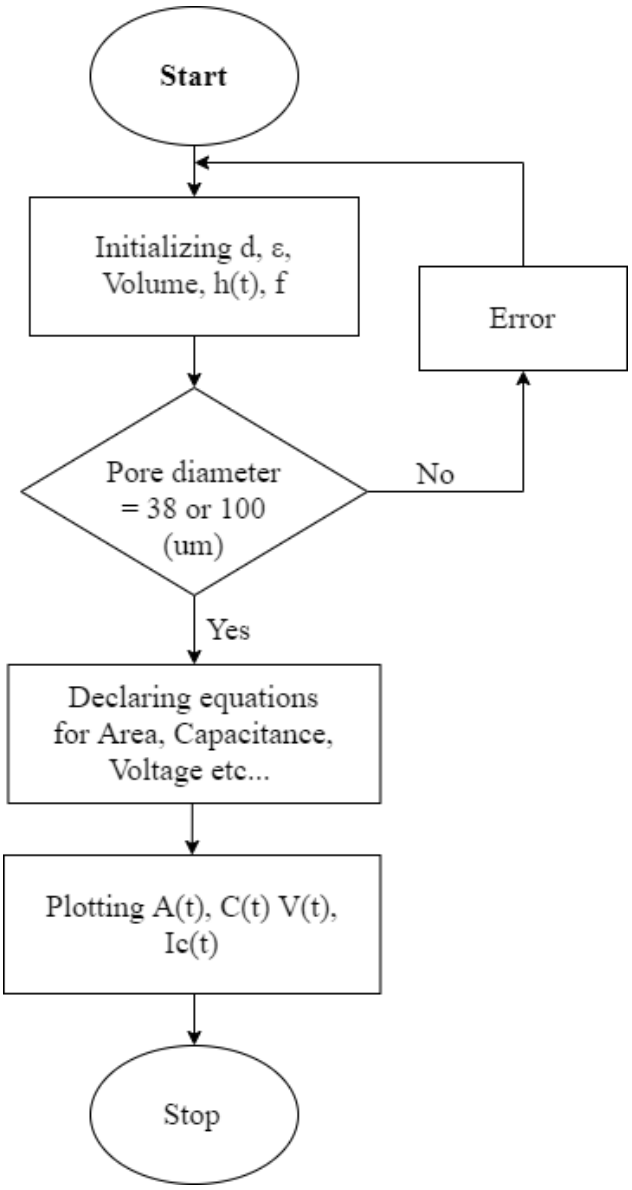

FIGURE 2.16. Flow chart/Algorithm for porous REWOD model

implementation code to estimate the area covered, capacitance, voltage, current and power are calculated.

The algorithm is different from the previous models. In this porous model, initialization block is same as planar and rough model but after the initializing block, a decision block is used to give input from the command window for the diameter of the pore. For porous design, if the input arguments are either 38 μm or 100 μm are accepted, else the code returns an error and starts again. After the decision block, the area, capacitance, and voltage

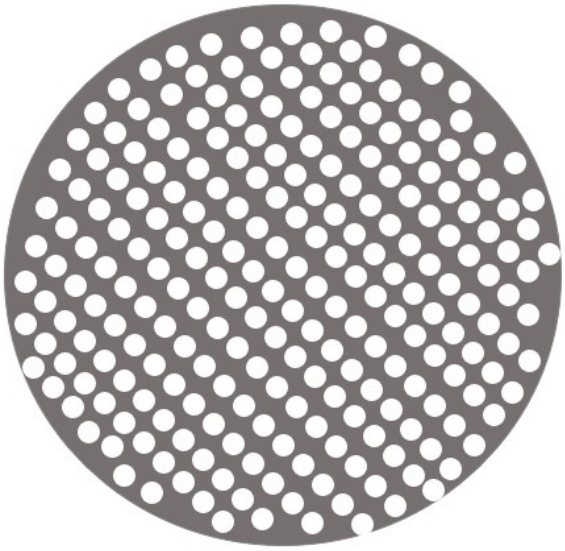

FIGURE 2.17. Top view of porous REWOD model bottom electrode

calculation are derived for plotting the waveform. Hence deriving the equation for area, capacitance, and voltage so that they are included in the code.

The lumped circuit shown in the Fig-2.18 is the electrical circuitry representation of the porous REWOD model. As observed in the figure, the resistor (R_s) is the source resistance of the electrodes and electrolyte. C_c is the constant capacitance that the electrolyte is always in contact with the electrode and $C(t)$ is the time-variant capacitance that the electrolyte covers when the electrodes are oscillating. R_L is the load resistance. From the circuit, the resultant capacitance is given as:

$$C = C_C + nC(t) = \frac{\epsilon_0 \epsilon_{eff} A_C}{d_1 + d_2} + \frac{\epsilon_0 \epsilon_{eff} n A(t)}{d_1 + d_2} \tag{2.37}$$

In the equation-2.37 A(t) and A_C are the area covered by the liquid where A(t) is the varying area of the liquid which is covered in the holes in the bottom electrode and A_c is the constant area covered by the liquid and this area is fixed.

$$A(t) = 2\pi r h(t) \tag{2.38}$$

The equation-2.38 is the area of the cylinder. The pores in the electrode is considered as cylinder. Using the area of the cylinder formula, the pore area (covered by the liquid) is

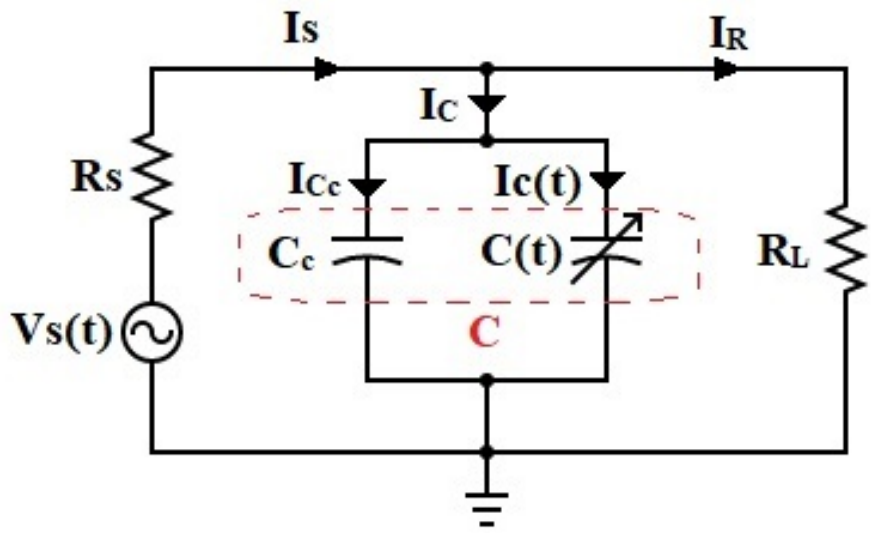

FIGURE 2.18. Voltage based lumped circuit model for porous REWOD design

calculated.

$$V_c(t) = \pi r^2 h(t)$$
$$V_c(t) = \frac{1}{2} r A(t) \tag{2.39}$$

The total volume of the liquid is the same as the planar and rough model i.e., 50 μm.But, the volume shown in the equation-2.39 is the volume of electrolyte covered in the pore. Due to the mechanical pressure the height of the liquid covered in the cylindrical hole varies so that it helps the amount of conduction takes place in the pore.

From these equation the varying capacitance can be calculated. In the equation-2.37 A_C is the area covered by the constant area that electrolyte covers. So, $A(t)$ is varying and that will show the different in the resultant capacitance. For voltage and current calculation it is calculated using the resultant capacitance (C(t)) and the derivation is as follows:

$$\frac{dA(t)}{dt} = 2\pi r \frac{dh(t)}{dt} \tag{2.40}$$

h(t) is the varying height that electrolyte cover in the cylinder. According to the measurements, the depth of the hole is 380 μm, so the liquid goes to and fro from 0 - 380 μm and the diameter of the hole is different for different electrodes (e.g: 38 μm and 100 μm).

It is shown in the fig-1.3 in that figure it clearly shows how the liquid droplet goes into the hole and also the area that the liquid covers.

$$\begin{aligned} \frac{dC(t)}{dt} &= \frac{\epsilon_0 \epsilon_{eff}}{d_1 + d_2} \frac{dA(t)}{dt} \\ \frac{dC(t)}{dt} &= \frac{(2\pi r)\epsilon_0 \epsilon_{eff}}{d_1 + d_2} \frac{dh(t)}{dt} \end{aligned} \tag{2.41}$$

The rate of change of capacitance is used to calculate the voltage and current for the porous-based REWOD energy harvester.

The circuit shown in the fig-2.18 is the voltage based lumped electric circuit for porous REWOD design. Focusing on that figure the current I_C is divided into two parts I_{C_c} current across constant capacitor C_c and $I_C(t)$ current across the varying capacitor C(t). From the equation-2.37 C=C_c+nC(t), the rate of change of equivalent capacitor ($\frac{dC}{dt}$) is

$$\begin{aligned} \frac{dC}{dt} &= \frac{dC_c}{dt} + n\frac{dC(t)}{dt} \\ \frac{dC}{dt} &= 0 + n\frac{dC(t)}{dt} \\ \frac{dC}{dt} &= n\frac{dC(t)}{dt} \\ \frac{dC}{dt} &= \frac{(2\pi rn)\epsilon_0 \epsilon_{eff}}{d_1 + d_2} \frac{dh(t)}{dt} \end{aligned} \tag{2.42}$$

As observed in the equation-2.42 $\frac{dC_c}{dt} = 0$ because it is time independent variable so there is no change in that capacitance. Hence the equation becomes $\frac{dC}{dt} = n\frac{dC(t)}{dt}$. Using $\frac{dC}{dt}$ and substituting in the V(t) derivation, we get the voltage equation for porous design.

$$V_s(t) = V_{sdc} + V_{ac}(t) I_R(t) = \frac{V(t)}{R_L} \tag{2.43}$$

$$Z(t) = R_s + Z_1(t) \tag{2.44}$$

$$Z_1(t) = X_C || R_L = \frac{X_C R_L}{X_C + R_L} \tag{2.45}$$

$$X_C = \frac{1}{2\pi f C} \tag{2.46}$$

$$I_S(t) = \frac{V_S(t)}{Z_1(t)} = I_C(t) + I_R(t) \tag{2.47}$$

$$V(t)(\frac{1}{Z_1(t)} - \frac{1}{R_L}) = V_{sdc}\frac{dC}{dt}$$

$$V(t)\frac{V_{sdc}\frac{dC}{dt}}{\frac{1}{Z_1(t)} - \frac{1}{R_L}} \tag{2.48}$$

$$I_c(t) = V_{sdc}\frac{dC}{dt}$$

This is the final voltage equation and current across the capacitor for the porous-based REWOD model. These equations will help in developing the mathematical model to simulate in MATLAB for realistic measurement of porous REWOD model.

2.3.3.1. Results and Simulation

A script has been developed for the REWOD porous model that the results could be relevant to the practical measured data. Using the formulas according to the derivation for capacitor, voltage, and current using them in developing the MATLAB-based code for comparing the amount of energy harvested to practically measured data. The fig-2.19 shows the comparison between the MATLAB measured capacitance and practically measured capacitance at different pour diameters. From the plot, it is evident that both practical and theoretical capacitance and nearly matching and from the theoretical plot the Capacitance at 38 μm pore diameter is 0.35 μF and for 100 μm pore diameter the capacitance gained is 0.1 μF. From the comparison, the average capacitance error at 38 μm pore diameter is 6% (94% accuracy) and similarly, for 100 μm pore diameter the average error is nearly 10% (90% accuracy).

The comparison between measured and simulated voltage plot is shown in the fig-2.20. From the plot it is clear that both the measured and simulated voltage is nearly same. From the simulation the output voltage for 38 μm design is varies from 0.9 - 3.3 V @ 1 - 5 Hz frequency respectively. Similarly for 100 μm design the voltage output is varies from 100 - 600 mV.

From the fig-2.21 it represents the power comparison for measured and simulated power. In 38 μm the power gained is varying from 5 - 55 μW and the average power is nearly 29.3

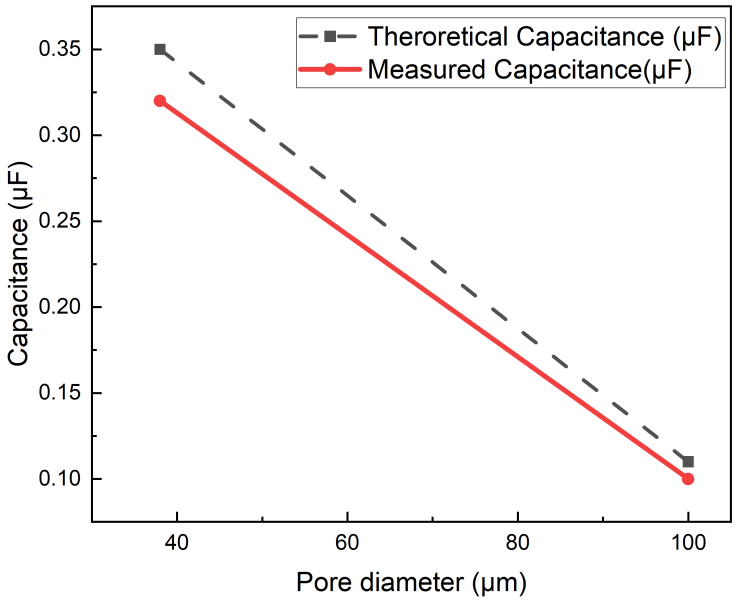

FIGURE 2.19. Capacitance comparison between MATLAB and measured measurement for porous REWOD model

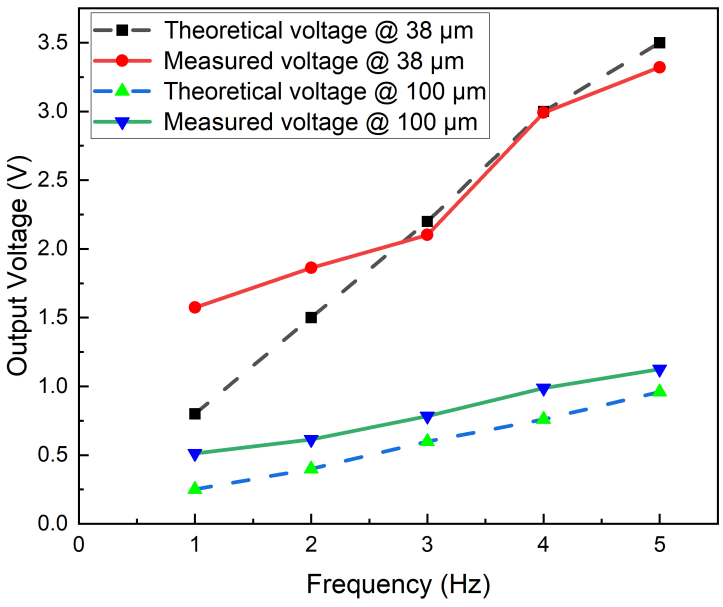

FIGURE 2.20. Voltage comparison between MATLAB and practical measurement

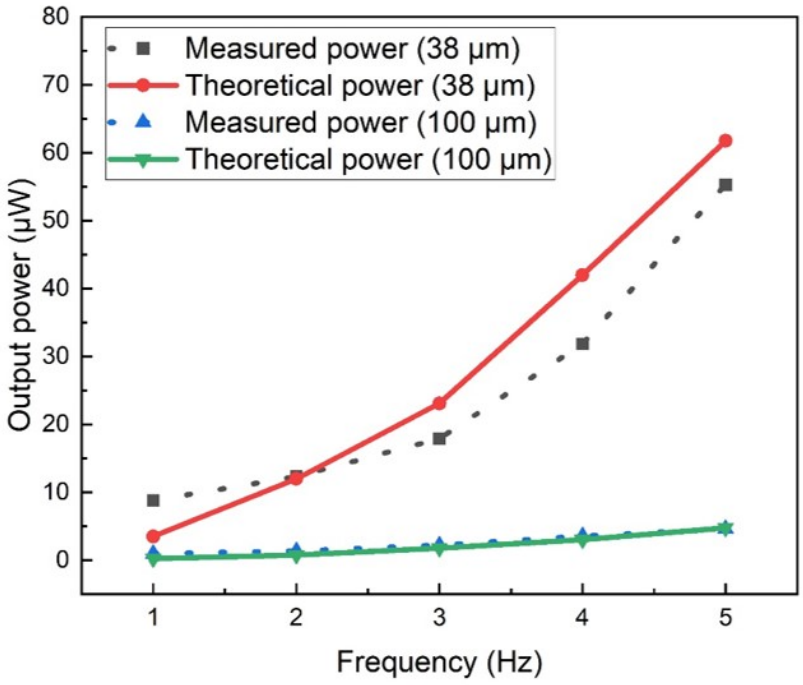

FIGURE 2.21. Power comparison plot between MATLAB and measured measurement for porous REWOD model

μW. The average error for this model is 25% (75% accuracy). Similarly, for 100 μm porous model the average power gained from the simulation model is 2.14 μW. Calculating the average error concerning measured data the error is nearly 20% which implies 80% accuracy. The higher error rate for both models is due to few parameters that are not included in the design. But, for further update, all the parameters including resistor modeling included in the modeling for higher accuracy.

From the table-2.1 it is clearly shown that the average power and average voltage gained by the porous 38 μm model is higher compared to others.

TABLE 2.1

Comparison between 3 REWOD model

REWOD models	**Capacitance**	**Voltage**	**Power output**
Planar model	6.5 nF	90 mV	4.66 nW
Rough model	0.97 μF	160 mV	54.4 nW
Porous model (100 μm)	0.10 μF	804 mV	2.14 μW
Porous model (38 μm)	0.35 μF	2.37 V	29.3 μW

CHAPTER 3

DESIGN OF RECTIFIER USING LTSPICE

3.1. Literature Review

The design of self-powered sensors has been developed in many fields and is very easy to use. However, there are few applications that are not suitable for low-voltage AC signals, so they need to be rectified into a constant DC signal. Few energy harvesters (such as REWOD) generate an AC signal with a very low frequency and low voltage range. Thus, a rectifier is designed to convert low-frequency alternating current into direct current. There has been many designs that implemented since many years for the rectifier that are used [**26**, **28**–**30**, **35**].

The rectifier is used to convert alternating current (AC) into direct current (DC). There are so many designs that are proposed for a rectifier among them The full-wave rectifier is an example. Consider a full-wave rectifier or bridge rectifier consists of P-N junction diodes as shown in the fig-3.1, operate at minimum 0.7 V voltage to conduct the diodes and this

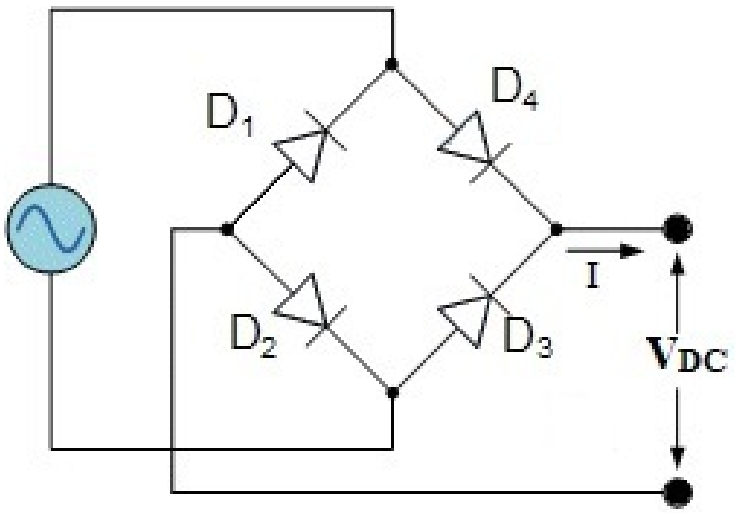

FIGURE 3.1. Full wave rectifier/bridge rectifier

rectifier is having power conversion efficiency (PCE) of nearly 81.2%. In a full-wave rectifier, two diodes are used, one diode is used to rectify the positive peak value, and the other diode is used to rectify the negative peak value. In this way, alternating current is converted to direct current. Similarly, in order to improve designs that operate under low frequency and voltage signals, a transistor-based rectifier was designed. The high-efficiency boost rectifier has a wide frequency operating range of 10 kHz-100 MHz. The designed rectifier by Suri achieved a power conversion efficiency (PCE) of 51% with 100 mV @ 7.25 MHz input signal, which makes it highly applicable for the inductive-coupling-based wireless power transfer applications for implantable sensors [**32**]. Jingmin et al. showed it achieves a very high efficiency of 95.5% at 0.2 V @ 100 Hz [**19**], the proposed technique by jingmin uses DTMOS, for which the body terminal is connected to the gate in a diode-connection form. This factor helps in rectifying the input voltage with wider dynamic control over the threshold voltage. Not only the frequency of the input signal but also the start-up voltage plays a major role in the efficient operation of the circuit. Similarly pointing to many limitations there is a requirement in designing a rectifier that operates at low-frequency voltage. In the paper, [**18**] explains the design of an efficient harvesting circuit explains the design of an RF - DC converter but, the design operates at very 700 MHz which is very high. Hence using different parameters and implementing a rectifier that operates at a very-low-frequency range of less than 5 Hz.

In this work a rectifier is design which will work at very low input frequency signal. So, designing a rectifier that operates at an input voltage of 100 mV and frequency range of 1-5 Hz.

3.2. Introduction to the Rectifier Design

As shown in Fig-3.2, This is a transistor-level implementation using NMOS transistors. With the help of cross-coupling capacitors, the design circuit converts AC voltage to boosted DC voltage. The output from the REWOD generator is provided as an input to the rectifier. The AC voltage signal generated by the planar REWOD model is around 100-250 mV with a frequency range of 1-5 Hz. The circuit consists of NMOS transistors

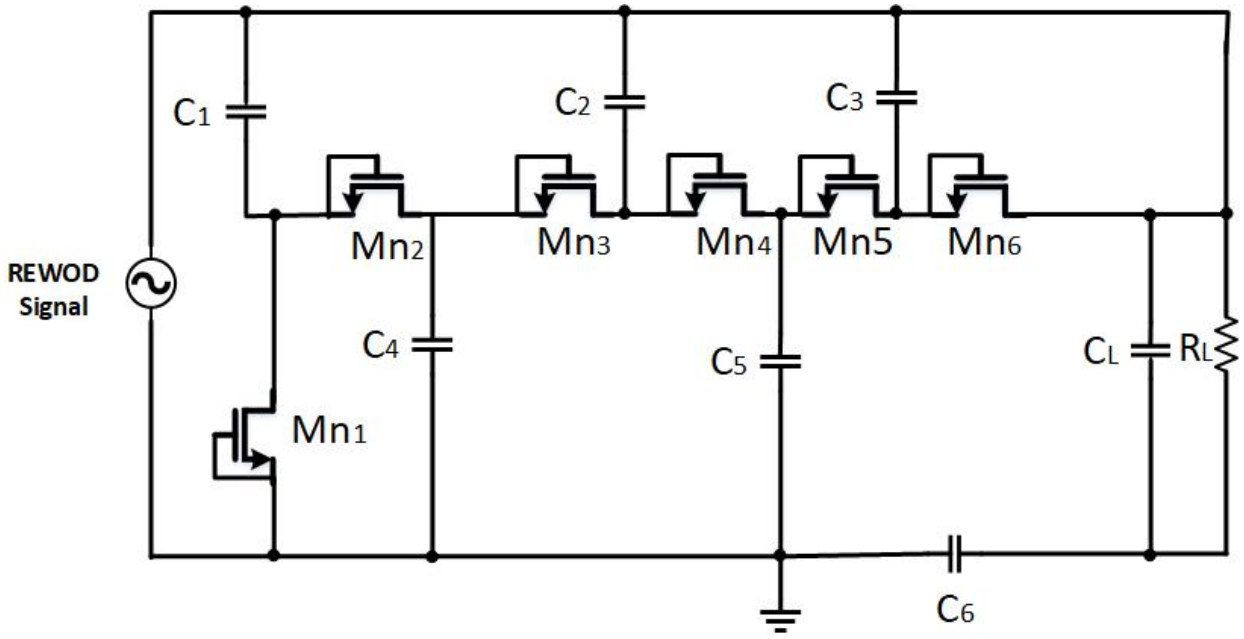

FIGURE 3.2. Proposed boost rectifier

where positive and negative peaks of the input AC signal are rectified by the circuit. During the positive cycle, Mn_1 is ON and Mn_2 is OFF so the positive cycle is rectified. Similarly, during the negative cycle, Mn_1 is ON and Mn_2 is OFF so the negative cycle is rectified, in this way both positive and negative cycles are rectified and cascaded to the next stage. During every stage, the DC output is boosted. First, in this work, the rectifier is designed in LTspice using commercial components. The rectifier is designed using transistors and lumped elements (capacitors and resistors). In the fragrance implementation, FDS6699S is used as a transistor. As shown in the Fig-3.2 the complete design of the rectifier is shown in the circuit. In this design AC input range of 100 mV - 2 V at a frequency range between 1-5 Hz is considered and tested the output response.A commercial component with an NMOS transistor FDS6699S is designed, and the circuit is designed using an NMOS transistor FDS6699S with a coupling capacitance of 1μF and a load resistance of 10 Mω.

3.2.1. Results and Simulation

In order to test the circuit, the input range is 100 mV - 2 V @ 1 -5 Hz frequency. Then, the result for the input power vs output power and input voltage vs output power is

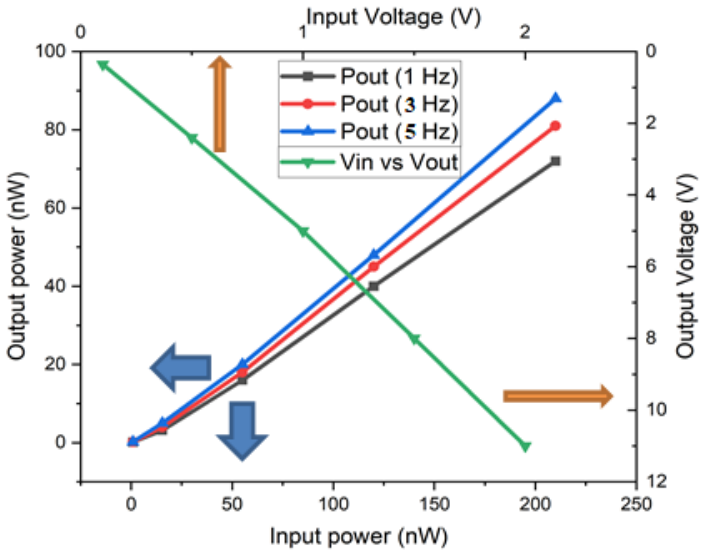

FIGURE 3.3. Plot between Pin vs Pout and Vin vs Vout

plotted in the Fig-3.3. It can be seen from the same figure that the voltage gain is very high even at 100 mV @ 1 Hz input signal The output voltage is close to 360 mV, and also for 2 V @ 1 Hz, the design has achieved 11V. From the Fig-3.4 this represents the plot between the input power vs power conversion efficiency (PCE) and from the plot, it can be evident that at 100 mV and 1 Hz frequency the PCE is nearly 17 % and for 2 V @ 1 Hz input, the efficiency is 35 %. While increasing the voltage the power conversion efficiency (PCE) also increases by observing the 2 V @ 5 Hz data point in the graph.

The output response of the input AC signal is completed by the rectifier design, and the result is appropriate. For the expansion of the project, the input comes from the REWOD output. Therefore, the AC input generated by REWOD was provided to the rectifier, and the voltage output and power conversion efficiency related to the REWOD input were tested. The results are as shown in the following plots. From the Fig-3.5 it can be observed that the output from the rectifier for 38 μm and 100 μm porous model. In the figure, it is clear that the voltage output range for 38 μm is varying from 2.9 - 6.7 V at a frequency range of 1 - 5 Hz. Similarly for 100 μm model the voltage range varies from 700 mv - 1.8 V.
Similarly from the fig-3.6 represents the output power and PCE (%) for 38 μm model. It has

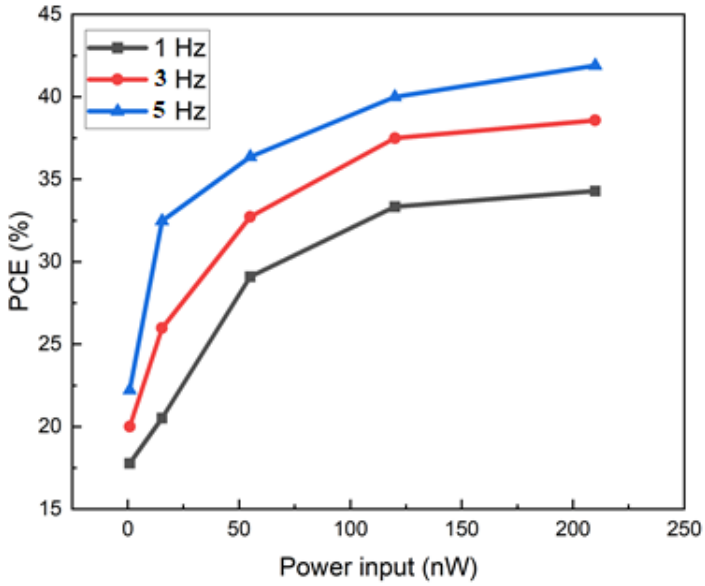

FIGURE 3.4. Plot between Pin vs PCE (%)

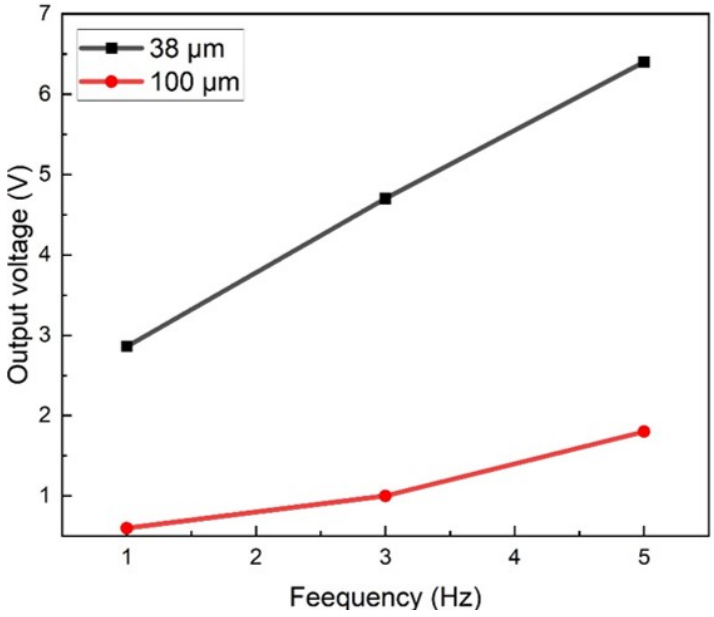

FIGURE 3.5. Plot between Vin vs Vout after REWOD input

gained nearly 27% accuracy from the rectifier. And from the fig-3.7 the PCE is nearly 15% for 100 μm model. The power consumption from the model is more from the design thereby, designing and implementing the circuit by minimizing the chip size. For miniaturization, the

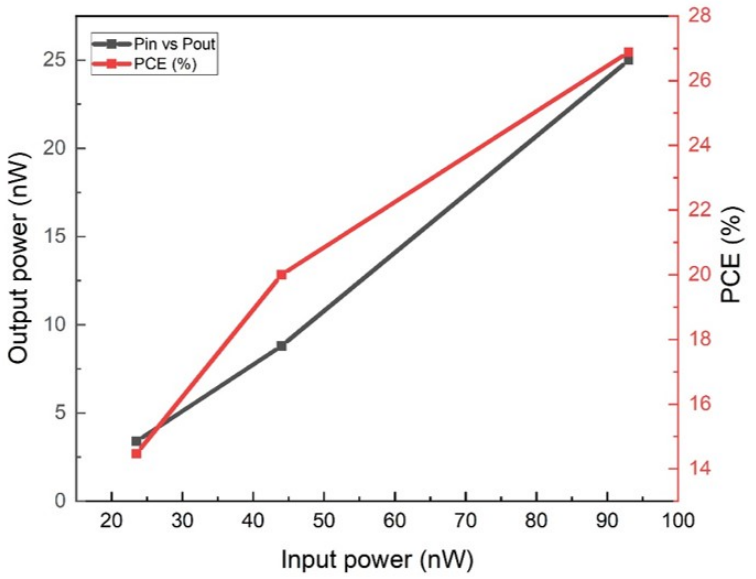

FIGURE 3.6. Plot between Pin vs Pout and PCE for 38 μm pore diameter

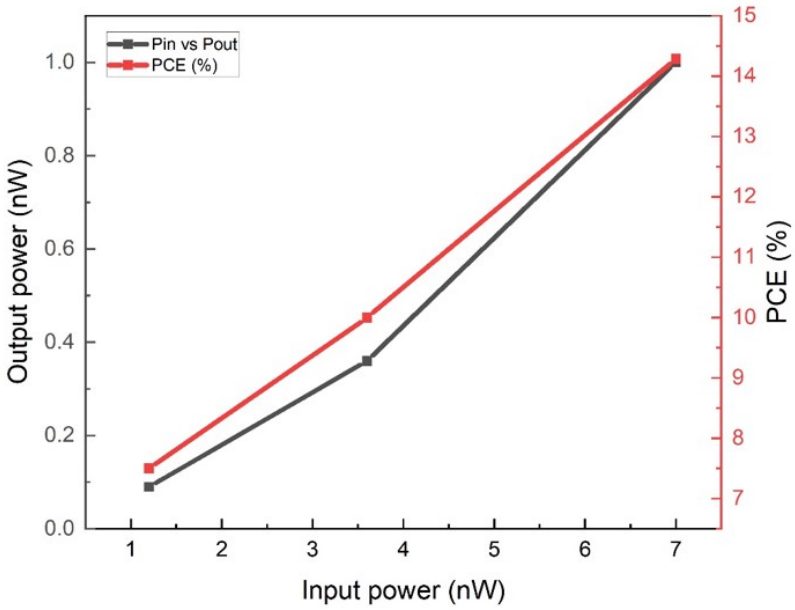

FIGURE 3.7. Plot between Pin vs Pout and PCE for 100 μm pore diameter

rectifier was designed and implemented in a 180 nm CMOS processor for more effectiveness.

CHAPTER 4

DESIGN OF RECTIFIER AND DC-DC BOOSTER USING CMOS 180 NM PROCESS

This entire chapter is reproduced from A. Gunti, D. K. Biswas, I. Mahbub, P. R. Adhikari and R. C. Reid, "Highly Efficient Rectifier and DC-DC Converter Designed in 180 nm CMOS Process for Ultra-Low Frequency Energy Harvesting Applications," 2020 IEEE 14th Dallas Circuits and Systems Conference (DCAS), 2020, pp. 1-5, with permission from IEEE. [1]

4.1. Literature Review

In the field of circuit design (VLSI), the miniaturization of circuits is being realized every day. Succeeding Moore's law, the chips are becoming very small, and the power consumed by the chips in the circuit also reducing. For the early basic circuit, it consumes about 3.3-5 V input voltage to operate previously, but due to the minimization and modernization of the upgraded size, the design power consumption is also reduced. Hence, the proposed rectifier is designing in 180 nm CMOS standards.

The design of voltage rectifiers is implemented by many researchers [**10**, **22**, **34**]. However, the same circuit as designed and explained in the previous section is used to implement the rectifier. A DC-DC boost converter is also used in the design. Therefore, the output of the rectifier is very low, and for few energy harvesting applications, the output needs to be increased. Therefore, the DC-DC boost rectifier is also designed together with the rectifier. Amongst many booster designs for DC-DC converter, the Dickson charge pump is one of the most popular architectures that is used as a DC-DC boost converter but the input voltage needs to be high because of the forward voltage requirement of traditional diodes. Hence, cross-coupled switched-capacitor circuits are better for low input voltage boosting [**4**]. Huan Peng proposed a charge pump circuit designed in a standard 0.18 μm CMOS process [**25**]. It consists of 6 stages, each with a 24 pF pumping capacitor the minimum start-up required is 350 mV output voltage rise from 0 to 2.04 V within 0.1 milliseconds,

[1] doi: 10.1109/DCAS51144.2020.9330671

making it not suitable for input voltage amplitude of 100 mV. A similar problem can be observed for the work present in [**27**], where the PCE dropped by more than 50% when the input voltage is reduced from 500 mV to 220 mV. But at 500 mV the VCE and PCE are 90% and also for this design, the minimum operating voltage is 380 mV. Similarly, for the DC-DC voltage booster, the charge pump circuit is used to regulate the output DC voltage. Apart from that, Buck-boost converters are also a better technique for DC-DC conversion. An inductor-less DC-DC converter is used for micro-power harvesting, it provides output regulation at 1.4 V with 58% power conversion efficiency but, the minimum input voltage for this design is 270 mV [**31**]. When connected to a sinusoidal source of 3.3 V peak amplitude, it allows improving the overall power efficiency by 11% compared to the best recently published results given by a gate cross-coupled-based structure due to its efficiency and input voltage is not suitable for low voltage design [**14**].

4.2. Design Architecture in 180 nm CMOS Process

The frequency (1-5 Hz) and amplitude (95-890 mV) of the AC signals collected from the REWOD generator for human motion activities (such as walking and running) are very low. The low-frequency signal needs to be rectified and the rectified DC voltage (V_{rect}) needs to be boosted to a certain constant voltage using pump circuits or converters according to the system requirement without using any external sources. A simple block diagram is shown in Fig-4.1 for a better understanding of the concept. In Fig-4.1 the working of REWOD is shown, it explains that the AC signal generated by REWOD is connected to the rectifier, which is designed in such a way that it can rectify even the ultra-low frequency signal. The rectified output is fed to a DC-DC boost converter, which can boost the rectified voltage to operate some sensors and sensors. Explaining rectifier and DC-DC boost circuit in-depth as followed.

a) Rectifier: As shown in the Fig-3.2 This is a transistor-level implementation using NMOS transistors. With the help of cross-coupling capacitors, the design circuit converts AC voltage to DC voltage. The output of the REWOD generator is provided as the input of the rectifier.

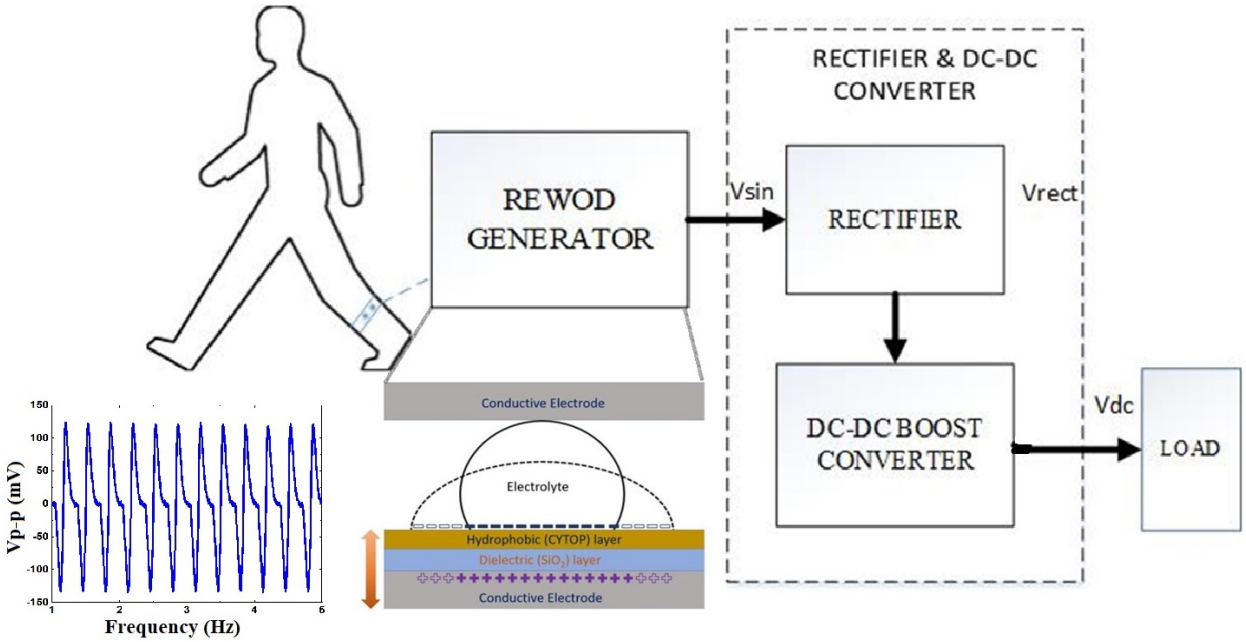

FIGURE 4.1. Block diagram for proposed energy harvesting circuitry

The AC voltage signal generated by REWOD is about 100-250 mV, and the frequency range is 1-10 Hz. As mentioned in the previous section, this circuit consists of all NMOS transistors, in which the positive and negative peaks of the input AC signal is rectified by the circuit. During the positive cycle, Mn1 is ON, and Mn2 is OFF so the positive cycle is rectified. Similarly, during the negative cycle, Mn1 is ON and Mn2 is OFF so the negative cycle is rectified, in this way both positive and negative cycles are rectified and cascaded to the next stage.At each stage, the DC output will rise. With the help of a 180 nm CMOS process using the ideal capacitance such that the time constant is much larger than the input signal period, so the capacitance is taken as 1 nF and NMOS transistors of Length (L) are 180 nm and width (W) is 220 nm with a load resistance of 10 MΩ according to the current requirement. Thereafter, that rectified voltage from the rectifier (Vrect) is provided to the 5-stage DC-DC voltage booster.

b) DC-DC booster: The circuit shown in Fig- 4.2 is a voltage doubler circuit or a charge pump. So, adding multiple stages of this circuit and gain our required output DC voltage. In this design 5-stages of the cross-coupled switched capacitor are cascaded. Each stage is made of two latched CMOS pairs (M_{n1}, M_{p1}, M_{n1}, M_{p1}). The transfer capacitors of each

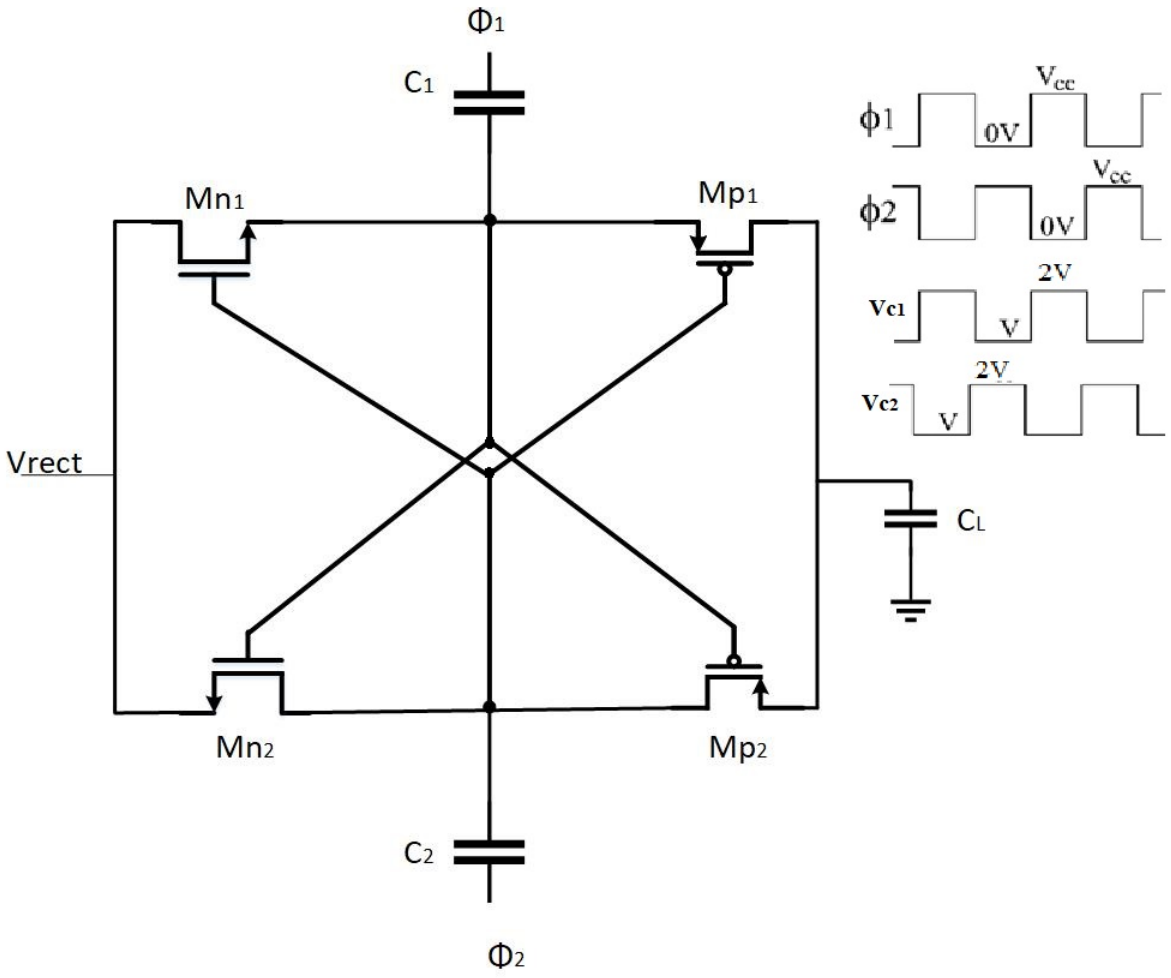

FIGURE 4.2. DC-DC Booster

stage are alternately charged to the voltage of the previous stage and then boosted by V_{rect} to charge the next stage at a higher voltage. During the first half cycle when ϕ_1 is high ($\phi_2(= phi_1)$ is low) transistors (M_{n2}, M_{p1}) are ON (V_{C1}= V_{ϕ_1}, V_{C2}=0), and transistors (M_{n1}, M_{p2}) are OFF, transfer capacitor C_2 is charged to V_{rect} through M_{N2}, while transfer capacitor C_1 is boosted to V_{rect} +V_{ϕ_1} through M_{p1}. During the second half cycle, transistors (M_{n1}, M_{p2}) are turned ON, and transistors (M_{n2}, M_{p1}) are turned OFF, transfer capacitor C_1 is charged to V_{rect}, while transfer capacitor C_2 is boosted to V_{ϕ_1} + V_{rect}. Once NMOS (M_{n1}) has enough gate-source voltage then PMOS (M_{p2} starts charging and similarly for M_{n2} and M_{p2}. thereby, the output transfers to the next stage. The clock frequency in the design is 1k Hz, which is generated by a multi-vibrator or ring oscillator.

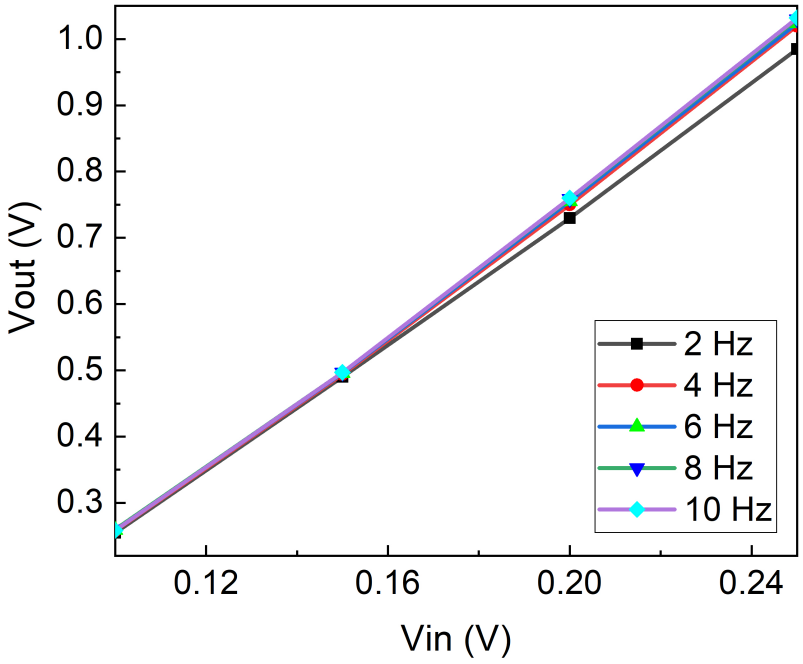

FIGURE 4.3. V_{out} vs V_{in} for the proposed rectifier

4.3. Simulation Results

The simulation results of the rectifier and the DC-DC converter circuit are discussed in this section. Fig- 4.3 presents the simulation results between V_{out} vs V_{in} of the rectifier. As can be seen from the figure, the output voltage boosts the input voltage linearly at a frequency range of 1 - 10 Hz. The minimum voltage to conduct this circuit is 80 mV and the output voltage at 80 mV is 190 mV.

Fig- 4.4 is the plot between voltage conversion efficiency vs. input voltage at different frequencies from 1-10 Hz.

In the same figure, the plot lines are voltage conversion efficiency for 2Hz, 4Hz, 6Hz, 8Hz, 10Hz frequencies respectively with an input voltage range of 100 mV - 250 mV AC. At this range the output voltage range is 250 mV - 1.1 V DC.

$$VCE_n = \frac{V_{out_n}}{V_{in}} \times 100\% \tag{4.1}$$

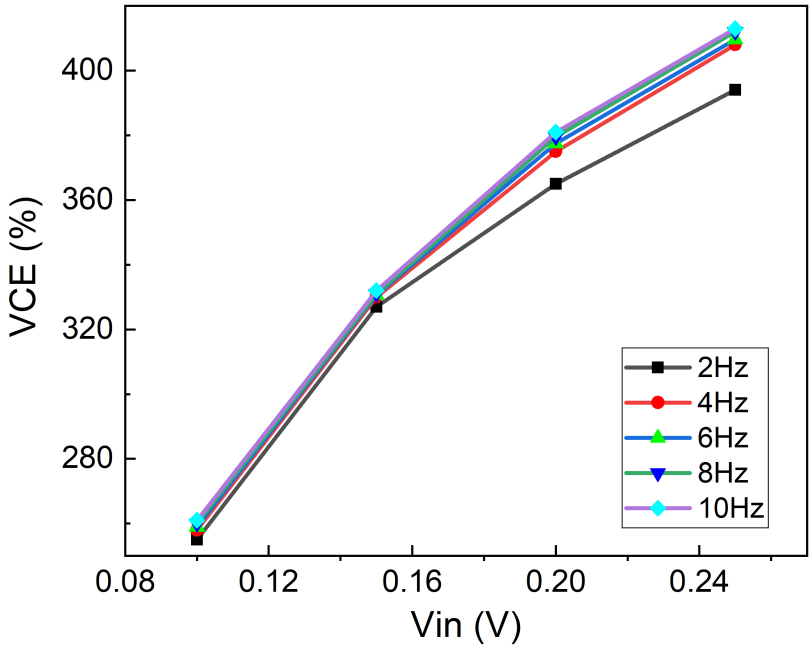

FIGURE 4.4. Voltage conversion efficiency vs. input voltage of the proposed rectifier

Where V_{out_n} is the output voltage at different frequencies, V_{in} is the input voltage and equation (4.1) is the formula for the voltage conversion efficiency. It is used in the calculation after the results are obtained from the simulation. The results are shown in Fig-4.4. It can be observed that when input voltage increases the voltage conversion efficiency increases. So, from the fig- 4.4, at a higher input voltage of 250 mV @ 10 Hz, it can be observed with a higher voltage conversion efficiency of nearly 420 %. And the VCE is range is 250-420%.

From the Fig- 4.5, we can observe the power conversion efficiency vs P_{in} of the rectifier. At 250 mV @ 10 Hz frequency the PCE is 15%. The figure is plotted between different input voltages at different frequencies. To achieve more power efficiency, Adjusting W, L and number of fingers of MOSFET.

In Fig- 4.6 it is clear that at 100 mV of AC the output DC voltage is 1.18 V. Increasing the input voltage linearly increases the output DC voltage. The output voltage range at 100-

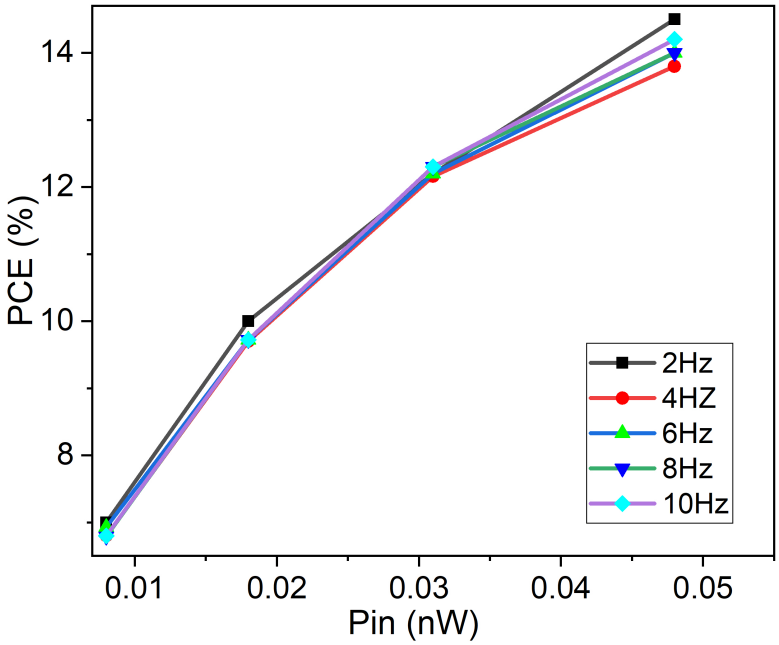

FIGURE 4.5. PCE vs. P_{in} of the proposed rectifier

250 mV input AC voltage is 1.2-2.1 V DC.

4.7. Fig- 4.7 is the plot between Voltage conversion efficiency vs. input AC voltage (100 - 250 mV) from the REWOD. At 250 mV @ 10 Hz of the frequency, the average output DC voltage is 2.1 V, which is high enough to be used as a supply voltage for the load like some sensor and transducers. The VCE range is between 840-1220%.

$$PCE_n = \frac{P_{out_n}}{P_{in}} \times 100\% \tag{4.2}$$

The above equation (4.2) represents the power conversion efficiency at different frequencies(n). Fig- 4.8 shows the plot between power conversion efficiency(P_{out}) and input power(P_{in}). For the corresponding input according to Vin range of 100 - 250 mV the PCE range 15-30%. From the observation of both VCE and PCE, It is evident that at 100 mV input with 2 Hz frequency both VCE and PCE efficiencies are 1200% and 30% respectively.

TABLE I: summarise the performance summary and comparisons of this work rectifier and charge-pump and the state-of-the-art designs. The boost converter in [**15**] is having

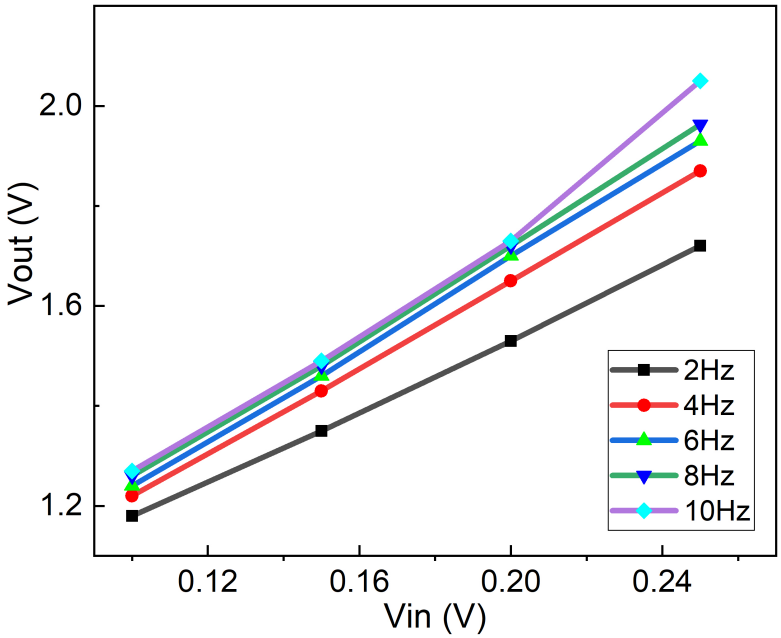

FIGURE 4.6. V_{out} vs. V_{in} for the rectifier and DC-DC boost converter

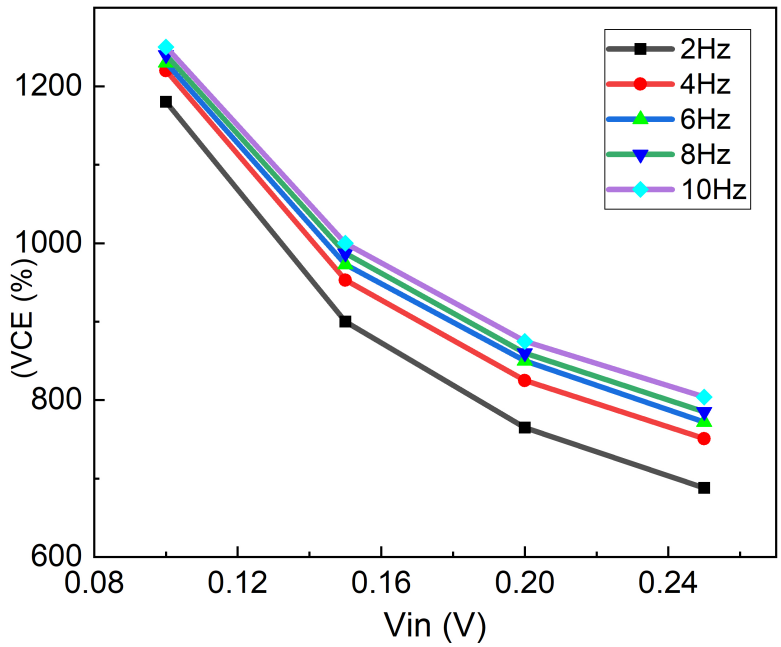

FIGURE 4.7. VCE vs. Vin of both rectifier and DC-DC boost converter

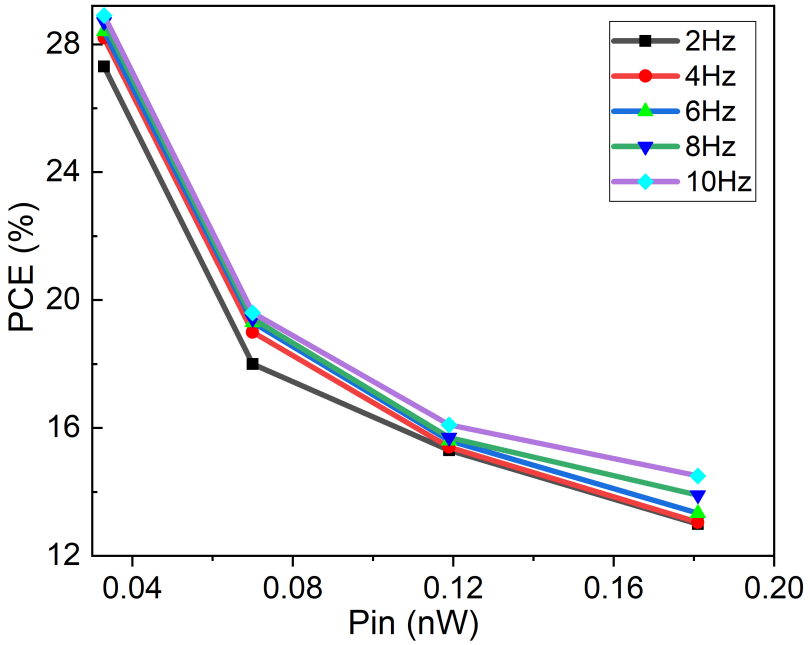

FIGURE 4.8. PCE vs. Pin for rectifier and DC-DC boost converter

TABLE 4.1

Performance summary and comparisons

Ref, Year	**Mechanism**	**Input voltage** (mV)	**Output voltage**	**VCE**	**PCE**
[**15**], 2015	Boost converter	300	1.1V	367%	39%
[**32**], 2019	Boost Rectifier (10k-100MHz)	200	2.03V	1015%	51%
[**19**], 2016	Rectifier (10Hz-1kHz)	200	181 mV	90.5%	90.5%
This work	Booster & Rectifier(1-10Hz)	100	1.2V	1180%	30%

less power efficiency and also the operating voltage is more. Considering [**32**] the frequency range is very high furthermore, it is designed in 130 nm process. The rectifier used in [**19**] is operated with very high efficiency at low voltage. However, it is not used as a boost rectifier

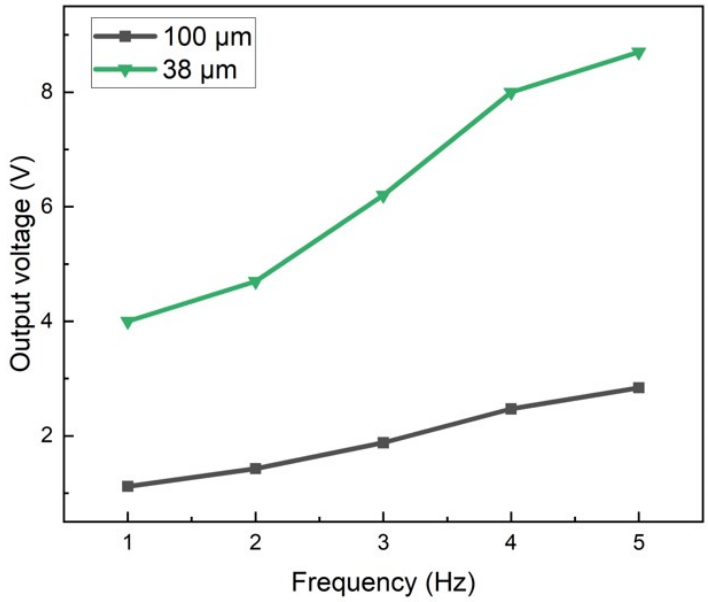

FIGURE 4.9. Cadence plot between Vin vs Vout after REWOD input

due to its voltage conversion efficiency. Considering the overall performance the proposed circuit achieves the low voltage operation at low frequency with effective output efficiency. This result is for testing the circuit for converting AC-DC and DC-DC boosting at low frequency signal. For further extension, REWOD generated AC signal is used as an input and testing the design for the performance analysis and voltage comparison. So, taking REWOD generated signal as rectifier input and analysed results are as shown.

Considering porous sample data i.e., 38 μm and 100 μm porous model as the input to the rectifier in the first case when the number of pores or holes having a diameter of 100 μm the output voltage range is 1.12 V to 2.84 V at an input frequency range of 1 - 5 Hz. The voltage plot is shown in the fig-4.9. Now, the power output and power conversion efficiency curves seen from Figure 1 are 1, 2, 3, 4, and 5 Hz, respectively, which are 15, 16.2, 19, 20.6, and 21, respectively. In the second case, consider the REWOD output for 38 μm diameter and feed it to proposed rectifier. The rectifier output voltage is 4 - 8.7 V which varies high compared to 100 μm. And PCE is 27 - 34.5% @ 1 - 5 Hz frequency respectively. While

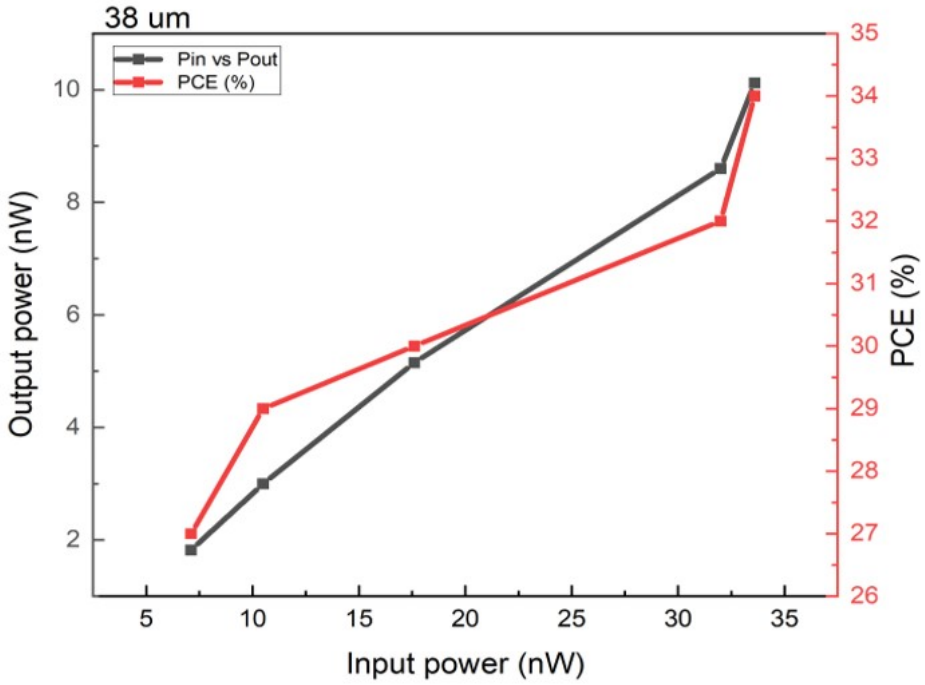

FIGURE 4.10. Cadence plot between Pin vs Pout and PCE after REWOD 38 μm pore input

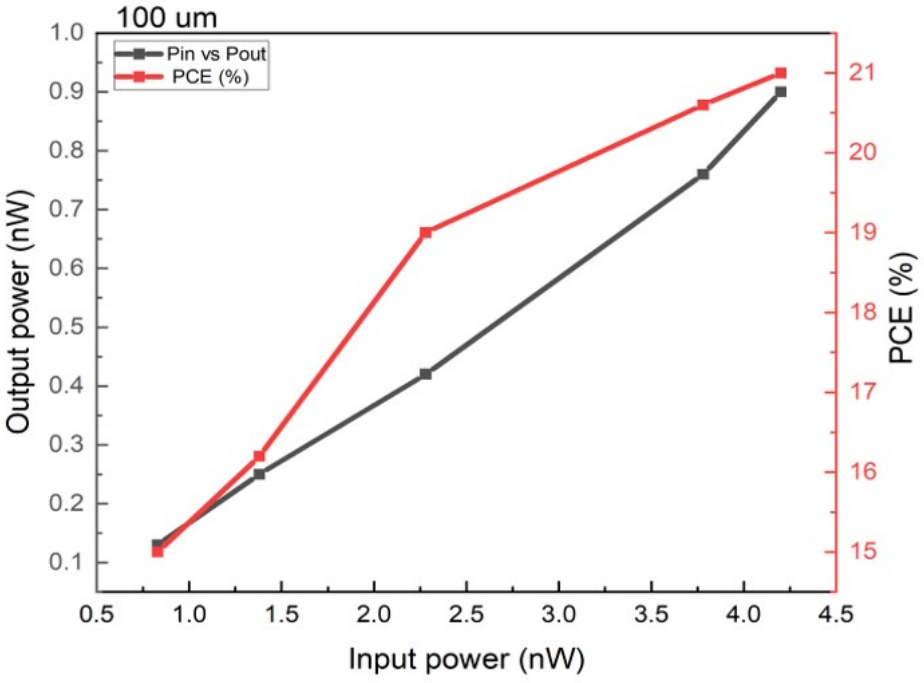

FIGURE 4.11. Cadence plot between Pin vs Pout and PCE after REWOD 100 μm pore input

comparing the results to the previous cases output voltage and PCE is high for 38 μm. And the comparison plot for output voltage is shown in the fig-4.9 and PCE plot is shown in the fig-4.10.

CHAPTER 5

FUTURE SCOPE AND CONCLUSION

With the help of MATLAB script, three different REWOD modeling are performed. From the observation the porous model has the higher output power and also the higher output voltage. By comparing both simulation and measured modeling the results are nearly same. But while calculating the error rate, simulated plots have high error rates. This can be minimize by including all the parameters including air capacitance, resistance modeling and capturing the exact inter-facial area covered by the liquid will help in getting higher accuracy.

Similarly from the low energy harvesting circuitry, a rectifier using commercial components and properly working at a low input voltage of 100 mV @ 1 - 5 Hz frequency. And when the REWOD generated output is injected to the proposed rectifier the output varies from 3 - 6.7 V for 38 μm porous model with 15 - 27% power conversion efficiency respectively. similarly, it has gained 0.7 - 1.8 V voltage with power conversion efficiency of nearly 8 - 14% for 100 μm model. Further these models are designed in the PCB using ALTIUM software and practically measuring the response.

Additionally, Using 180 nm CMOS technology standards a 3-stage boost rectifier and a 5-stage DC-DC boost converter are designed. As part of the work a very-low AC voltage of 100 mV is converted and boosted into 1.2 V DC voltage and 250 mV of AC voltage input is converted into 2.1 V DC voltage, validating the design approach in terms of efficiency and optimization. Hereby, the self-generated current from the REWOD generator is effectively converted and boosted into appropriate DC voltage which is applicable for various harvesting circuits. With the REWOD generated output the rectifier has gain the voltage range of 2 - 8.7 V with PCE varies from 27 - 34.5% respectively for 38 μm. Whereas, for 100 μm design the voltage rectified is 1.1 - 2.4 V with PCE varies from 15 - 21%. From comparing the result from both Ltspice and 180 nm CMOS process it is clear that the PCE and voltage output are higher for 180 nm design.

REFERENCES

[1] Pashupati Adhikari, Nishat Tarannum Tasneem, Russell Reid, and Ifana Mahbub, *Electrode and electrolyte configurations for low frequency motion energy harvesting based on reverse electrowetting*, Scientific Reports 11 (2021).

[2] Pashupati R Adhikari, Nishat T Tasneem, Dipon K Biswas, Russell C Reid, and Ifana Mahbub, *Reverse electrowetting-on-dielectric energy harvesting integrated with charge amplifier and rectifier for self-powered motion sensors*, ASME International Mechanical Engineering Congress and Exposition, vol. 84560, American Society of Mechanical Engineers, 2020, p. V008T08A035.

[3] Bowen An, Xianzhang Wang, Yang Xu, and Robert L Jackson, *Deterministic elastic-plastic modelling of rough surface contact including spectral interpolation and comparison to theoretical models*, Tribology International 135 (2019), 246–258.

[4] Andrea Ballo, Alfio Dario Grasso, and Gaetano Palumbo, *A review of charge pump topologies for the power management of iot nodes*, Electronics 8 (2019), no. 5, 480.

[5] Mallika Bariya, Hnin Yin Yin Nyein, and Ali Javey, *Wearable sweat sensors*, Nature Electronics 1 (2018), no. 3, 160–171.

[6] Jun Chen and Zhong Lin Wang, *Reviving vibration energy harvesting and self-powered sensing by a triboelectric nanogenerator*, Joule 1 (2017), no. 3, 480–521.

[7] Xu-rui Chen, Tong-qing Yang, Wei Wang, and Xi Yao, *Vibration energy harvesting with a clamped piezoelectric circular diaphragm*, Ceramics International 38 (2012), S271–S274.

[8] Young-Man Choi, Moon Gu Lee, and Yongho Jeon, *Wearable biomechanical energy harvesting technologies*, Energies 10 (2017), no. 10, 1483.

[9] Ulysse Côté-Allard, Gabriel Gagnon-Turcotte, François Laviolette, and Benoit Gosselin, *A low-cost, wireless, 3-d-printed custom armband for semg hand gesture recognition*, Sensors 19 (2019), no. 12, 2811.

[10] Peyman Nejat Dehkordi, Sayed Vahid Mir-Moghtadaei, and Noushin Ghaderi, *A high*

power conversion efficiency cmos rectifier using lc resonator technique for energy harvesting applications, 2019 27th Iranian Conference on Electrical Engineering (ICEE), IEEE, 2019, pp. 290–294.

[11] Yuji Gao, Hiroki Ota, Ethan W Schaler, Kevin Chen, Allan Zhao, Wei Gao, Hossain M Fahad, Yonggang Leng, Anzong Zheng, Furui Xiong, et al., *Wearable microfluidic diaphragm pressure sensor for health and tactile touch monitoring*, Advanced Materials 29 (2017), no. 39, 1701985.

[12] Xinjian Gu and Yiyun Huang, *The modelling and simulation of a rough surface*, Wear 137 (1990), no. 2, 275–285.

[13] Minjeong Ha, Seongdong Lim, and Hyunhyub Ko, *Wearable and flexible sensors for user-interactive health-monitoring devices*, Journal of Materials Chemistry B 6 (2018), no. 24, 4043–4064.

[14] S. S. Hashemi, M. Sawan, and Y. Savaria, *A high-efficiency low-voltage cmos rectifier for harvesting energy in implantable devices*, IEEE Transactions on Biomedical Circuits and Systems 6 (2012), no. 4, 326–335.

[15] Hugo Hernández and Wilhelmus Van Noije, *Fully integrated boost converter for thermoelectric energy harvesting in 180 nm cmos*, Analog Integrated Circuits and Signal Processing 82 (2015), no. 1, 17–23.

[16] Tsung-Hsing Hsu, Supone Manakasettharn, J Ashley Taylor, and Tom Krupenkin, *Bubbler: a novel ultra-high power density energy harvesting method based on reverse electrowetting*, Scientific reports 5 (2015), no. 1, 1–13.

[17] DH Huynh, TC Nguyen, PD Nguyen, CD Abeyrathne, Md S Hossain, R Evans, and E Skafidas, *Environmentally friendly power generator based on moving liquid dielectric and double layer effect*, Scientific reports 6 (2016), no. 1, 1–10.

[18] K. Ibrahim, E. A. El Ghanam, M. Ali, L. Albasha, and N. Qaddoumi, *Efficiency analysis of harvester circuits*, 2013 IEEE 20th International Conference on Electronics, Circuits, and Systems (ICECS), 2013, pp. 799–802.

[19] Wang Jingmin, Yang Zheng, Zhu Zhangming, and Yang Yintang, *An ultra-low-voltage*

rectifier for pe energy harvesting applications, Journal of Semiconductors 37 (2016), no. 2, 025004.

[20] Stanislaw Kucharski and Grzegorz Starzynski, *Study of contact of rough surfaces: Modeling and experiment*, Wear 311 (2014), no. 1-2, 167–179.

[21] Chao Li, Shan Cong, Zhengnan Tian, Yingze Song, Lianghao Yu, Chen Lu, Yuanlong Shao, Jie Li, Guifu Zou, Mark H Rümmeli, et al., *Flexible perovskite solar cell-driven photo-rechargeable lithium-ion capacitor for self-powered wearable strain sensors*, Nano Energy 60 (2019), 247–256.

[22] Seyed Mohammad Noghabaei, Rafael L Radin, Yvon Savaria, and Mohamad Sawan, *A high-efficiency ultra-low-power cmos rectifier for rf energy harvesting applications*, 2018 IEEE International Symposium on Circuits and Systems (ISCAS), IEEE, 2018, pp. 1–4.

[23] Jihun Park, Joohee Kim, So-Yun Kim, Woon Hyung Cheong, Jiuk Jang, Young-Geun Park, Kyungmin Na, Yun-Tae Kim, Jun Hyuk Heo, Chang Young Lee, et al., *Soft, smart contact lenses with integrations of wireless circuits, glucose sensors, and displays*, Science advances 4 (2018), no. 1, eaap9841.

[24] Young-Geun Park, Sangil Lee, and Jang-Ung Park, *Recent progress in wireless sensors for wearable electronics*, Sensors 19 (2019), no. 20, 4353.

[25] Huan Peng, Nghia Tang, Youngoo Yang, and Deukhyoun Heo, *Cmos startup charge pump with body bias and backward control for energy harvesting step-up converters*, IEEE Transactions on Circuits and Systems I: Regular Papers 61 (2014), no. 6, 1618–1628.

[26] C. Peters, J. Handwerker, D. Maurath, and Y. Manoli, *An ultra-low-voltage active rectifier for energy harvesting applications*, Proceedings of 2010 IEEE International Symposium on Circuits and Systems, 2010, pp. 889–892.

[27] Christian Peters, Jonas Handwerker, Dominic Maurath, and Yiannos Manoli, *A sub-500 mv highly efficient active rectifier for energy harvesting applications*, IEEE Transactions on Circuits and Systems I: Regular Papers 58 (2011), no. 7, 1542–1550.

[28] Mohd Anuar Rosli, Sohiful Anuar Zainol Murad, and Mohd Nazrin Md Isa, *Review*

of ac-dc rectifier circuit based on complementary metal-oxide semiconductor for radio frequency energy harvesting system, Proceedings of the Electronic and Green Materials International Conference, Surabaya, Indonesia, vol. 30, 2015.

[29] A. Shareef, W. L. Goh, S. Narasimalu, and Y. Gao, *A rectifier-less energy harvesting interface circuit for low-voltage piezoelectric transducers*, 2018 IEEE International Symposium on Circuits and Systems (ISCAS), 2018, pp. 1–5.

[30] ———, *A rectifier-less ac–dc interface circuit for ambient energy harvesting from low-voltage piezoelectric transducer array*, IEEE Transactions on Power Electronics 34 (2019), no. 2, 1446–1457.

[31] Yi-Chun Shih and Brian P Otis, *An inductorless dc–dc converter for energy harvesting with a 1.2-muw bandgap-referenced output controller*, IEEE Transactions on Circuits and Systems II: Express Briefs 58 (2011), no. 12, 832–836.

[32] Ramaa Saket Suri, Nishat T Tasneem, and Ifana Mahbub, *Low-power highly efficient voltage-boosting rectifier for wide-band inductively-coupled power telemetry*, 2019 United States National Committee of URSI National Radio Science Meeting (USNC-URSI NRSM), IEEE, 2019, pp. 1–2.

[33] Geoffrey H Tison, José M Sanchez, Brandon Ballinger, Avesh Singh, Jeffrey E Olgin, Mark J Pletcher, Eric Vittinghoff, Emily S Lee, Shannon M Fan, Rachel A Gladstone, et al., *Passive detection of atrial fibrillation using a commercially available smartwatch*, JAMA cardiology 3 (2018), no. 5, 409–416.

[34] Amad Ud Din, Muhammad Kamran, Waqar Mahmood, Khursheed Aurangzeb, Abdulaziz Saud Altamrah, and Jong-Wook Lee, *An efficient cmos dual switch rectifier for piezoelectric energy-harvesting circuits*, Electronics 8 (2019), no. 1, 66.

[35] H. Wang, Y. Tang, and A. Khaligh, *A bridgeless boost rectifier for low-voltage energy harvesting applications*, IEEE Transactions on Power Electronics 28 (2013), no. 11, 5206–5214.

[36] Fei Xing, Yang Jie, Xia Cao, Tao Li, and Ning Wang, *Natural triboelectric nanogenerator*

based on soles for harvesting low-frequency walking energy, Nano Energy 42 (2017), 138–142.

[37] Yangyiwei Yang, Shuai Wang, Peter Stein, Bai-Xiang Xu, and Tongqing Yang, *Vibration-based energy harvesting with a clamped piezoelectric circular diaphragm: analysis and identification of optimal structural parameters*, Smart Materials and Structures 26 (2017), no. 4, 045011.

[38] Wei Zhou, Jin-yuan Tang, Yan-fei He, and Cai-chao Zhu, *Modeling of rough surfaces with given roughness parameters*, Journal of Central South University 24 (2017), no. 1, 127–136.